Appendix E

Supplementary Information for Chapter 6

E.1.1 Materials and Methods

All manipulations were carried out using standard Schlenk or glovebox techniques under an N_2 atmosphere. Solvents were deoxygenated and dried by thoroughly sparging with N_2, followed by passage through an activated alumina column in a solvent purification system by SG Water, USA LLC. Nonhalogenated solvents were tested with sodium benzophenone ketyl in tetrahydrofuran (THF) to confirm the absence of oxygen and water. Deuterated solvents were purchased from Cambridge Isotope Laboratories, Inc.

Phenyl acrylate was purchased from Ambeed, degassed, and used without further purification. Cyclohexanedione monoethylene ketal (**1**) was purchased from TCI and used without further purification. All bases (DBU, Et_3N, pyridine, 2,6-lutidine) were purchased from Sigma Aldrich and distilled prior to use. $Sm(OTf)_3$, $Gd(OTf)_3$, and MgI_2 were purchased from Sigma–Aldrich. $Ir(ppy)_2(dtbbpy)[PF_6]$ was purchased from Strem and used without further purification. 3DPA2FBN (2,4,6-tris(diphenylamino)-3,5-difluorobenzonitrile) was purchased from Ambeed and used without further purification. 9,10-dihydroacridine was purchased from Combi-blocks and purified by sublimation prior to use. Hexamethylphosphoramide, ethylene glycol, and 2-(2-(2-methoxyethoxy)ethoxy)ethan-1-ol were purchased from Sigma Aldrich and degassed. Tetraheptylammonium iodide was purchased from TCI and dried at 100°C under dynamic vacuum for 16 hours. Tetrabutylammonium bromide was acquired from Strem and then dried by heating to 85°C for 48 hours under dynamic vacuum using P_2O_5 as a desiccant. 1-Butyl-1-methylpiperidinium (BMPipTFSI) was purchased from TCI chemicals and used without further purification.

$SmI_2(THF)_2$,[1] $phenH_2$,[2] BINAPO,[3] aminodiol (L*),[4] and [LutH]TFSI[5] were synthesized following literature procedures. HEH_2[6] synthesized following literature procedure and then dried by heating to 80 °C for 24 hours under dynamic vacuum using P_2O_5 as a desiccant.

The 2-MeTHF used was dried extensively prior to use in ketyl-olefin coupling experiments. Inhibitor-free solvent was refluxed over CaH_2 for 24 hours (under N_2 atmosphere) and distilled into a Strauss flask. This flask was brought into the glovebox,

where NaK was added, and the solvent was stirred for 24 hours. The solvent was then vacuum transferred into a fresh Strauss flask and stored over activated sieves.

E.1.2 Physical Methods

NMR: Nuclear Magnetic Resonance (NMR) measurements were recorded with a Varian 400 MHz spectrometer. ^{1}H NMR chemical shifts are reported in ppm relative to tetramethylsilane, using ^{1}H resonances from residual solvent as internal standards.

UV-Vis: Ultraviolet-visible (UV-vis) absorption spectroscopy measurements were collected with a Cary 50 UV-vis spectrophotometer using a 1 cm path-length quartz cuvette. All samples had a blank sample background subtraction applied. Temperature regulation for UV-Vis measurements was carried out with a Unisoku cryostat.

Electrochemistry: All electrochemical experiments were conducted using a CH instruments 600B electrochemical analyzer. A nonaqueous $Ag^{+/0}$ reference electrode (BASi) consisting of a silver wire immersed in 5 mM AgOTf in DME containing 0.2 M $^{n}Bu_4NPF_6$ separated from the working solution by a CoralPor® frit was used for all experiments. All reported potentials are referenced to the ferrocenium/ferrocene ($Fc^{+/0}$) couple used as an external standard. All CVs were carried out in an N_2-filled glovebox in a 20 mL scintillation vial fitted with a septum cap containing punched-out holes for insertion of electrodes. A glassy carbon disk (3 mm diameter) was used as the working electrode for all CVs. It was freshly polished with 1, 0.3, and 0.05 μm alumina powder water slurries, rinsed with water and acetone, and dried before use. A platinum wire was used as the auxiliary electrode for CVs. CVs are plotted using IUPAC convention. Unless otherwise noted, IR compensation was applied, accounting for 85% of the total resistance.

E.2. Catalytic ketone-olefin coupling reactions

E.2.1.1 Standard procedure in the absence of Ir-photocatalyst

In the glovebox, HEH_2 (40.4 mg, 160 μmol) was added as a solid to a Schlenk flask. 2-MeTHF (0.5 mL) was added to the flask. A freshly prepared stock solution of $SmI_2(THF)_2$ in 2-MeTHF (2.2 mg per mL, 4 mM) was added to the flask (1 mL added). A stock solution of the remaining organics: ketone (12.6 mg per mL; 80 mM), phenyl acrylate (22 μL per mL; 160 mM), and (when used) base, was prepared, and 0.5 mL was added to the reaction flask.

The color of SmI_2 (purple) rapidly changes to yellow upon the addition of the organic reagents. The reaction flask is sealed and brought out of the glovebox, where it is irradiated by two H160 PR Kessil™ 440 nm Blue LED lamps for 90 minutes in a water bath in a reflective dewar. The reaction was continuously stirred (1200 rpm). The temperature of the water bath was monitored and did not exceed 25 °C during the reaction.

Following completion of the reaction, the flask was opened to air, and 2 mL Et_2O was added. The contents of the flask was filtered through a silica plug into a vial containing a known amount of 1,3,5-trimethoxybenzene (TMB; ~7 mg). The reaction flask was washed with additional Et_2O (2x1 mL), and the washes were passed through the silica plug into the vial. The solvent was removed *in vacuo* and the products were taken up in $CDCl_3$ and analyzed by ^1H NMR integrating against the TMB standard.

Lactone product (**2**; 1,4,9-trioxadispiro[4.2.48.25]tetradecan-10-one) is detected by ^1H NMR with features matching literature spectra (Figure E.4).

Note: This reaction is very sensitive to solvent drying, and the CaH2/NaK method laid out in the general considerations is required. Similarly, the HEH2 must be dried as described. The reaction is sensitive to both water and air, as shown in Table E.2.

E.2.1.2 Standard procedure with an Ir-photocatalyst

In the glovebox, $Ir(ppy)_2(dtbbpy)[PF_6]$ (0.36 mg, 0.4 μmol) was dissolved in THF and added to a Schlenk flask, and the solvent was removed *in vacuo*, depositing a thin film. Following this HEH_2, $SmI_2(THF)_2$ and organics were added as described in **S2.1.1**

E.2.2 Yields for ketone-olefin coupling reactions

Table E.1. Yields of individual catalytic experiments.

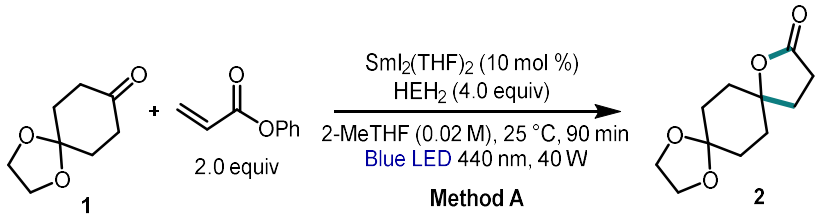

Entry	Variation from standard conditions	Yield lactone	Ketone recovery
A1	None	81%	14%
A2	None	74%	13%
A3	None	75%	15%
A4	None	73%	14%
Entry 1, Table 6.1A	None	76±3%	14±1%
A5	No light	5%	89%
A6	No light	4%	93%
Entry 2, Table 6.1A	No light	4±1%	91±2%
A7	No Sm	<1%	102%
A8	No Sm	<1%	100%
Entry 3, Table 6.1A	No Sm	<1%	101±1%
A9	$SmOTf_3$ (10 mol%) MgI_2 (50 mol%) instead of SmI_2	59%	41%
A10	$SmOTf_3$ (10 mol%) MgI_2 (50 mol%) instead of SmI_2	60%	42%
Entry 4, Table 6.1A	$SmOTf_3$ (10 mol%) MgI_2 (50 mol%) instead of SmI_2,	60±1%	41±1%
A11	$GdOTf_3$ (10 mol%) MgI_2 (50 mol%) instead of SmI_2,	<1%	101%
A12	$GdOTf_3$ (10 mol%) MgI_2 (50 mol%) instead of SmI_2,	<1%	95%
Entry 5, Table 6.1A	$GdOTf_3$ (10 mol%) MgI_2 (50 mol%) instead of SmI_2	<1%	98±3%
A13	2 equiv pyr	72%	8
A14	2 equiv pyr	72%	10
Entry 6, Table 6.1A	2 equiv pyr	72±1%	9±1%
A15	2 equiv Et_3N	6%	79%
A16	2 equiv Et_3N	5%	72%
Entry 8, Table 6.1A	2 equiv Et_3N	5±1%	75±4%
A17	$phenH_2$ instead of HEH_2	<1%	37%
A18	$phenH_2$ instead of HEH_2	<1%	39%
Entry 9, Table 6.1A	$phenH_2$ instead of HEH_2	<1%	38±1%
A19	15 min reaction time	29%	63%
A20	15 min reaction time	29%	65%
Entry 10, Table 6.1A	15 min reaction time	29±1%	64±1%
A21	Ethyl acrylate instead of phenyl acrylate	36%	46%
A22	Ethyl acrylate instead of phenyl acrylate	25%	52%
Entry 11, Table 6.1A	Ethyl acrylate instead of phenyl acrylate	31±5%	49±3%

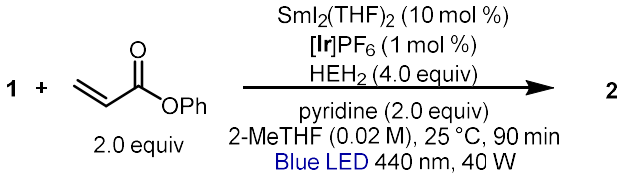

entry 10

Entry	Variation	Yield lactone	Ketone recovery
B1	None	87%	7%
B2	None	89%	6%
B3	None	89%	5%
B4	None	89%	4%
Entry 1, Table 6.1B	None	88.6±0.8%	5.7±1.1%
B5	No light	4%	94%
B6	No light	4%	92%
Entry 2, Table 6.1B	No light	4±1%	93±1%
B7	No Sm	<1%	89%
B8	No Sm	<1%	82%
Entry 3, Table 6.1B	No Sm	0%	86±3%
B9	$SmOTf_3$ (10 mol%) MgI_2 (50 mol%) instead of SmI_2	85%	14%
B10	$SmOTf_3$ (10 mol%) MgI_2 (50 mol%) instead of SmI_2	84%	13%
Entry 4, Table 6.1B	$SmOTf_3$ (10 mol%) MgI_2 (50 mol%) instead of SmI_2	85±1%	14±1%
B11	$GdOTf_3$ (10 mol%) MgI_2 (50 mol%) instead of SmI_2	6%	92%
B12	$GdOTf_3$ (10 mol%) MgI_2 (50 mol%) instead of SmI_2	6%	85%
Entry 5, Table 6.1B	$GdOTf_3$ (10 mol%) MgI_2 (50 mol%) instead of SmI_2	6±1%	88±4%
B13	No base	84%	8%
B14	No base	80%	8%
Entry 7, Table 6.1B	No base	82±2%	8±1%
B15	Et_3N instead of pyridine	13%	69%
B16	Et_3N instead of pyridine	17%	73%
Entry 8, Table 6.1B	Et_3N instead of pyridine	15±2%	71±2%
B17	$phenH_2$ instead of HEH_2	78%	0
B18	$phenH_2$ instead of HEH_2	76%	2
Entry 9, Table 6.1B	$phenH_2$ instead of HEH_2	77±1%	1±1%
B19	15 min reaction time	57%	43%
B20	15 min reaction time	66%	32%
Entry 10, Table 6.1B	15 min reaction time	61±4%	38±6%
B19	Ethyl acrylate instead of phenyl acrylate	59%	11%
B20	Ethyl acrylate instead of phenyl acrylate	56%	12%
Entry 11, Table 6.1B	Ethyl acrylate instead of phenyl acrylate	58±2%	12±1%

E.2.2.1 Quantification of additional organic products under standard conditions

While the work-up and detection method should account for ~100% of the ketone starting material, the limited solubility of HEH_2 in Et_2O and $CDCl_3$ and the low boiling point of phenyl acrylate result in some additional errors in these product yields. Figure E.1 presents approximate yields as integrated against a TMB standard for a reaction where care was taken to evaporate minimal phenyl acrylate.

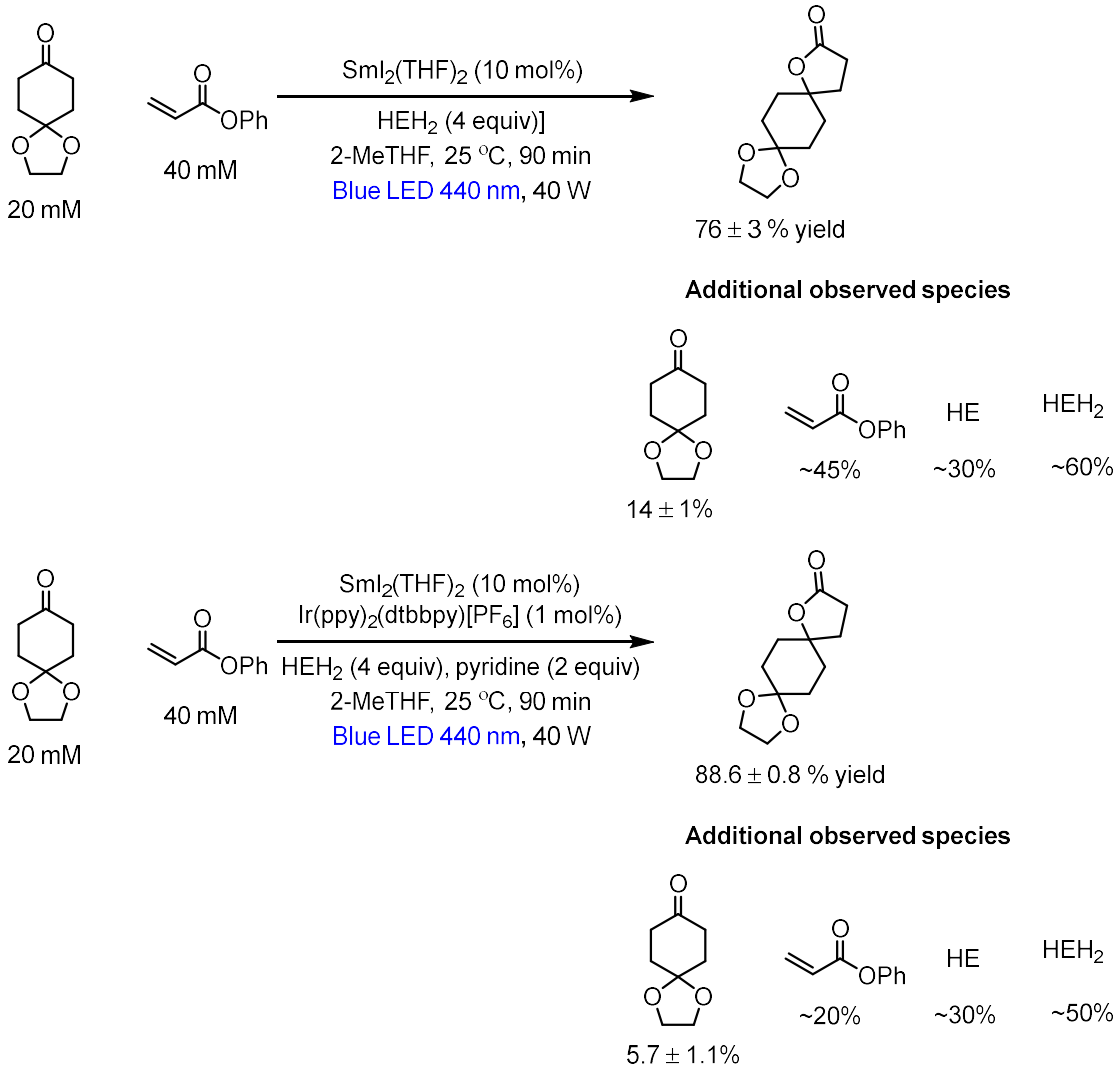

Figure E.1. Approximate yields of additional products under conditions without and with Iridium.

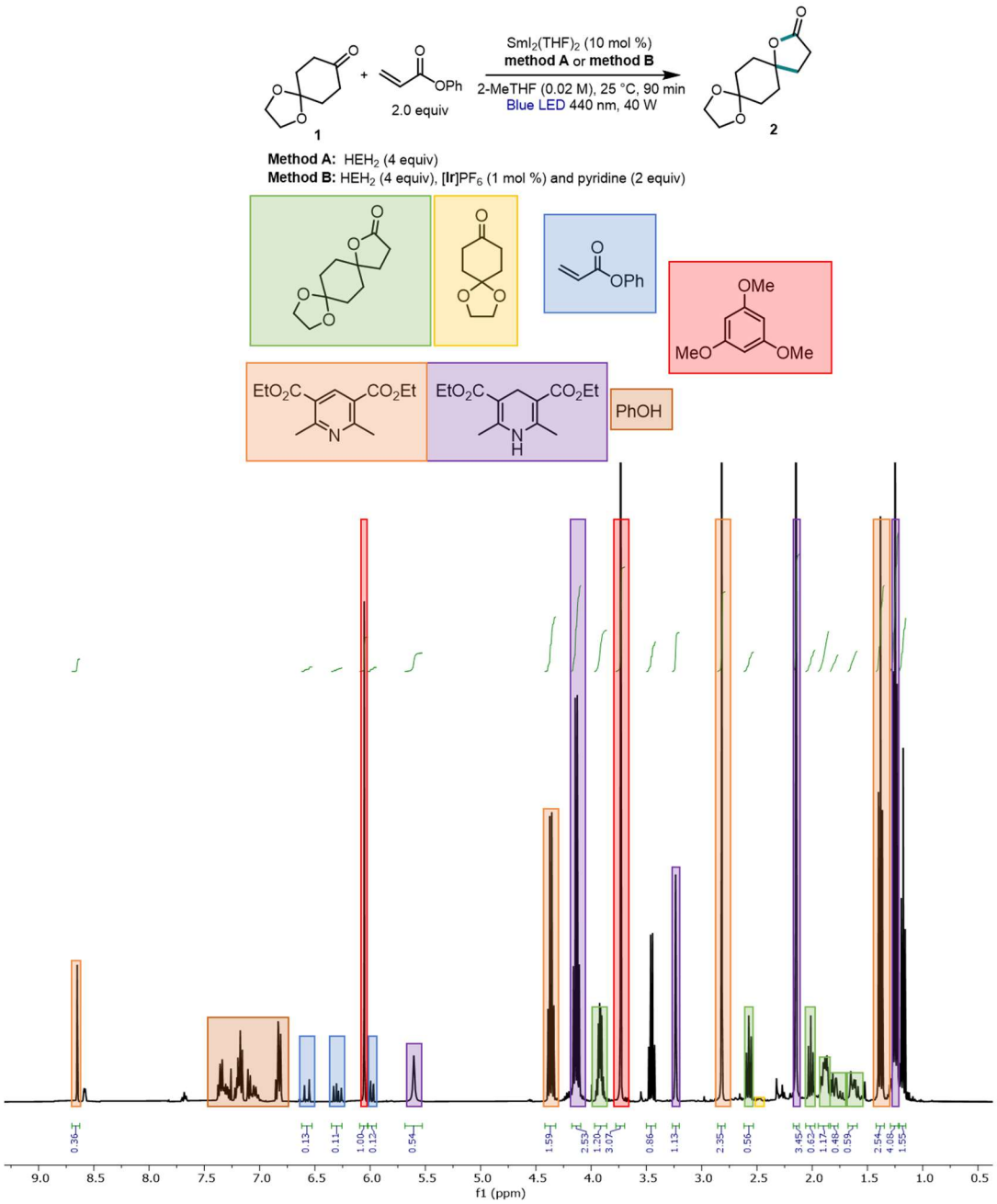

Figure E.2. ^{1}H NMR ($CDCl_3$ 7.26 ppm) of a typical crude reaction mixture reacting 1 with phenyl acrylate to produce 2 with key products/starting materials highlighted as indicated.

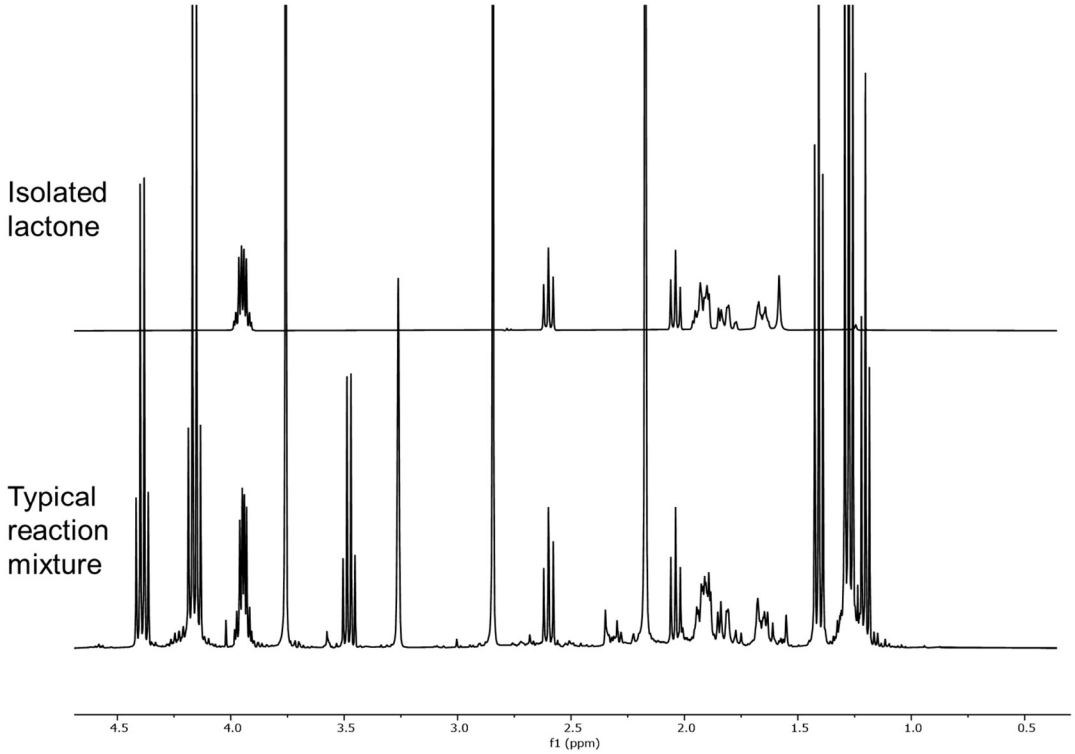

Figure E.3. Comparison of ^{1}H NMR of typical reaction spectra with authentic lactone product. ^{1}H NMR (400 MHz, $CDCl_3$): δ 4.00 – 3.90 (m, 4H), 2.60 (t, J = 8.5 Hz, 2H), 2.04 (t, J = 8.5 Hz, 2H), 1.97 – 1.88 (m, 4H), 1.82 (ddd, J = 17.5, 10.9, 4.0 Hz, 2H), 1.70 – 1.62 (m, 2H).

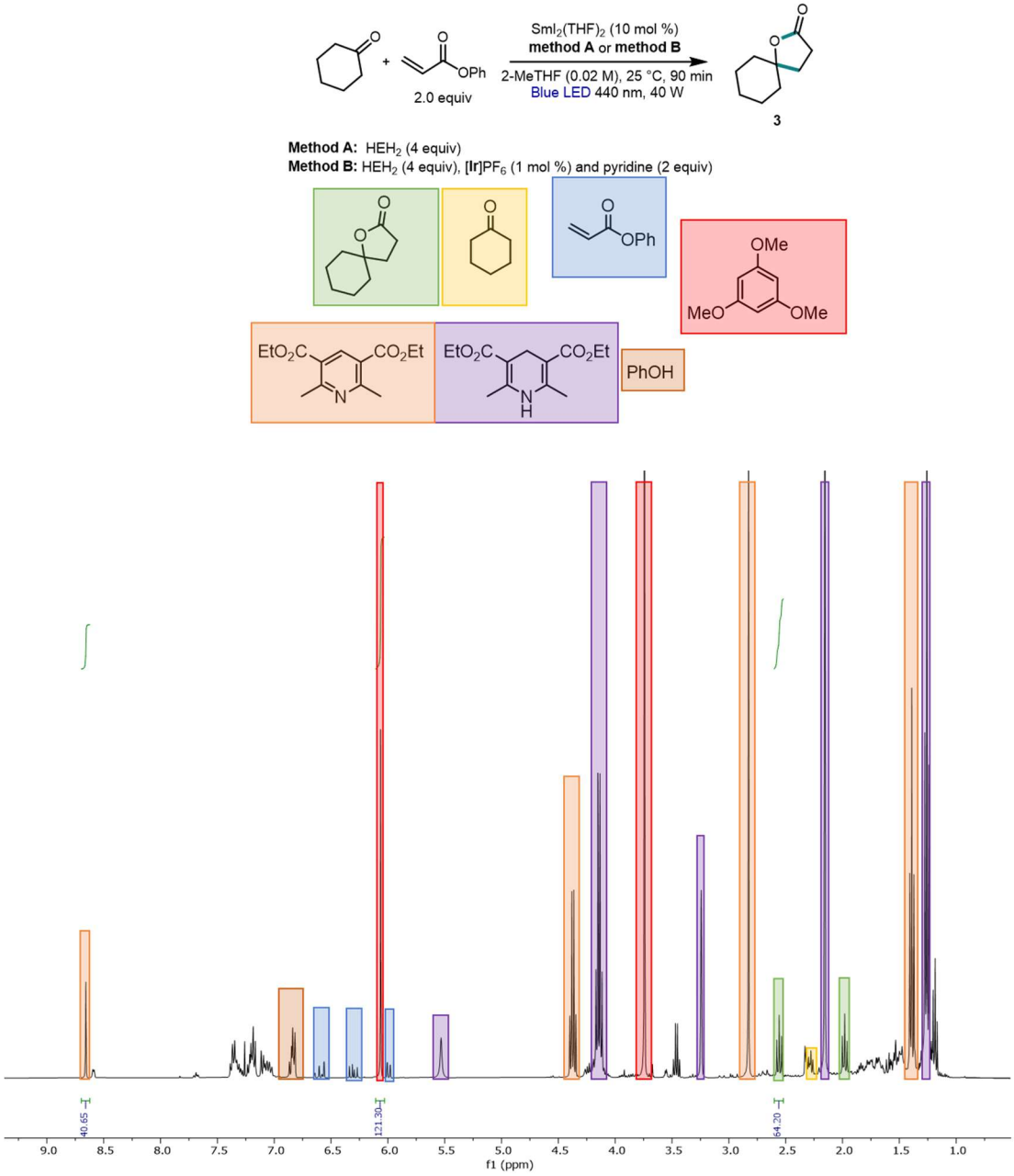

Figure E.4. ^{1}H NMR ($CDCl_3$ 7.26 ppm) of a typical crude reaction mixture reacting cyclohexanone with phenyl acrylate to produce 3 with key products/starting materials highlighted as indicated. The lactone product 3 matched previous reports.[5]

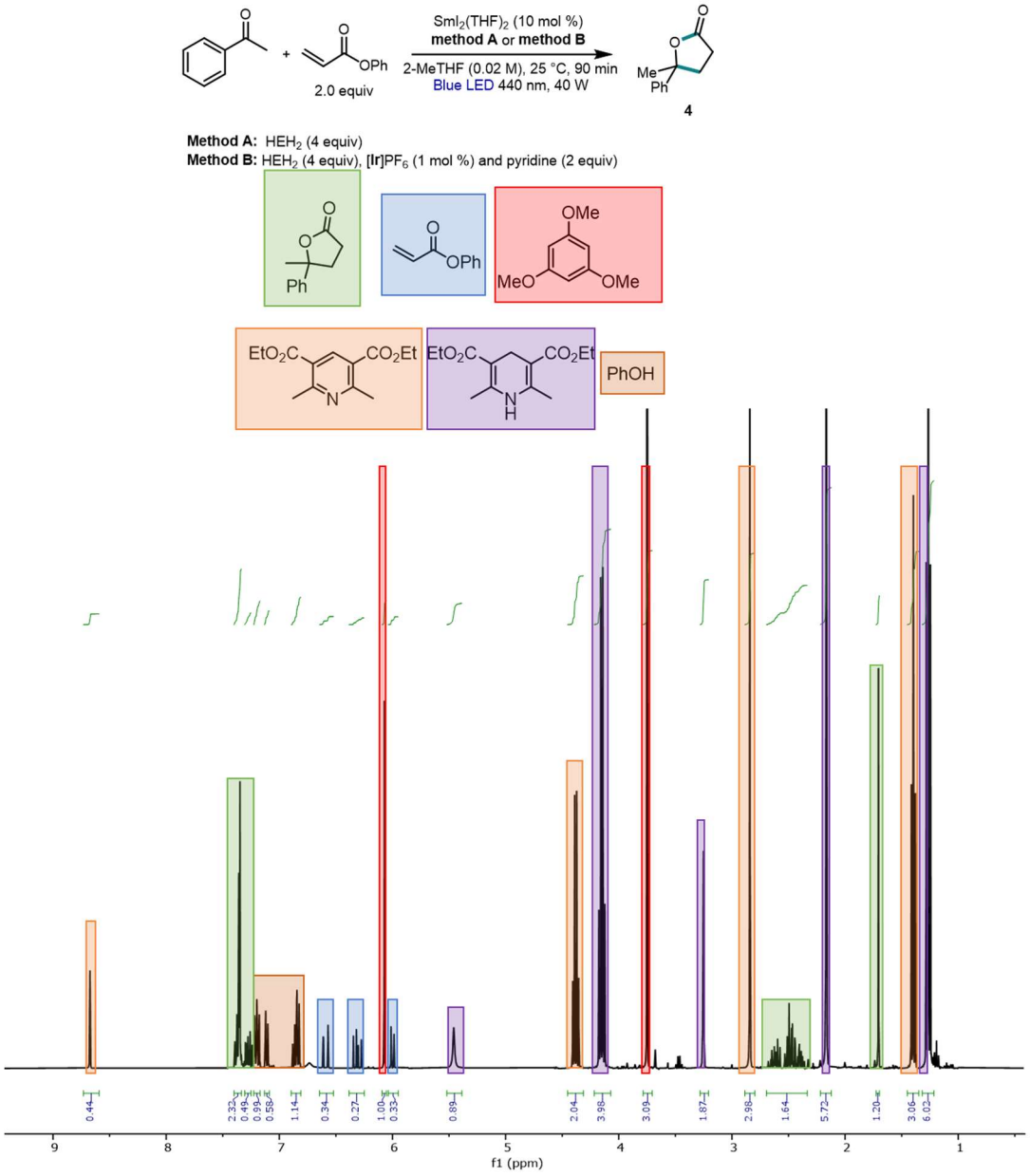

Figure E.5. ^{1}H NMR ($CDCl_3$ 7.26 ppm) of a typical crude reaction mixture reacting acetophenone with phenyl acrylate to produce 4 with key products/starting materials highlighted as indicated. The lactone product 4 matched previous reports.[5]

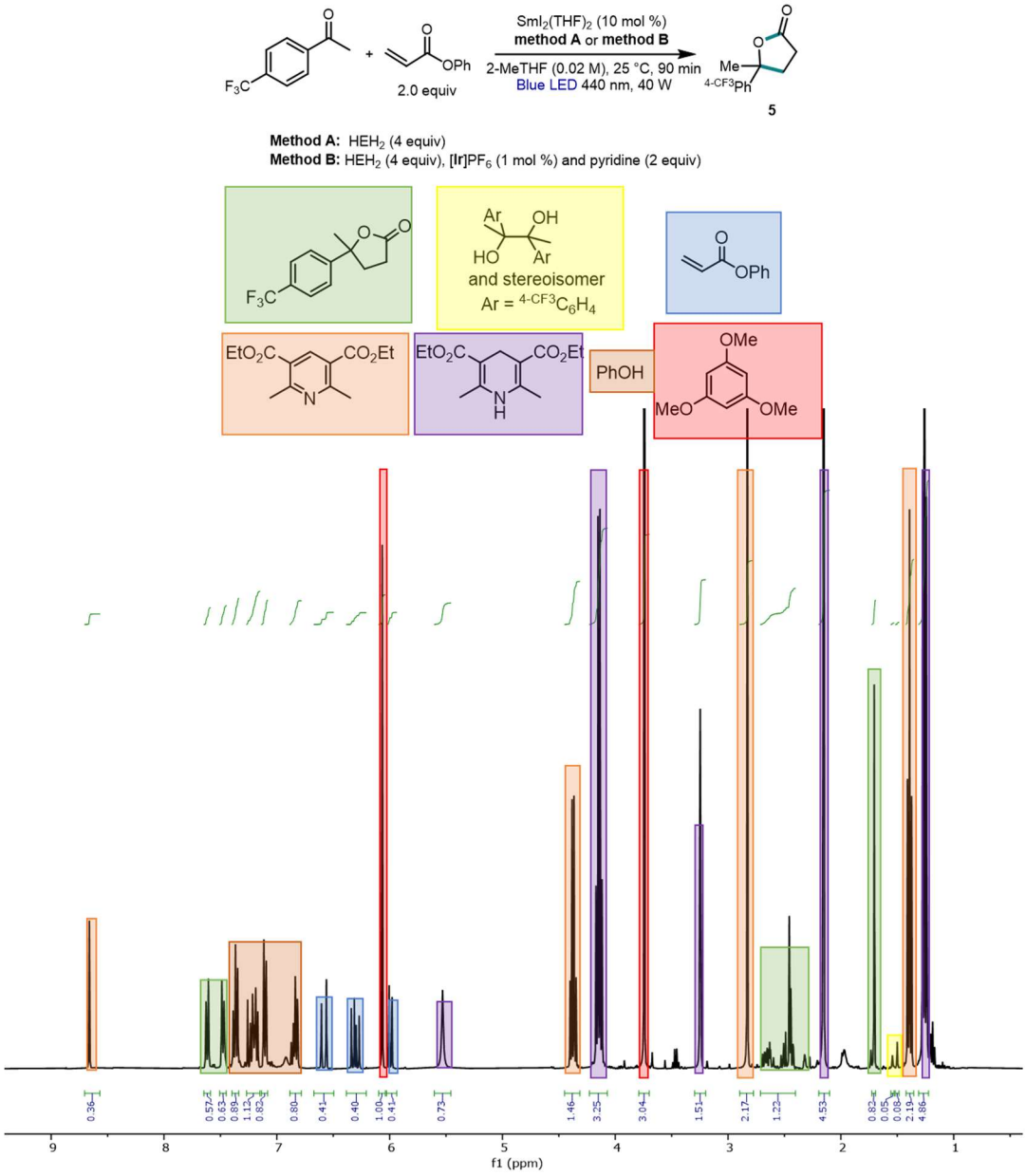

Figure E.6. ^{1}H NMR ($CDCl_3$ 7.26 ppm) of a typical crude reaction mixture reacting 4-trifluoromethyl acetophenone with phenyl acrylate to produce 5 with key products/starting materials highlighted as indicated. The lactone product 5 matched previous reports.[5]

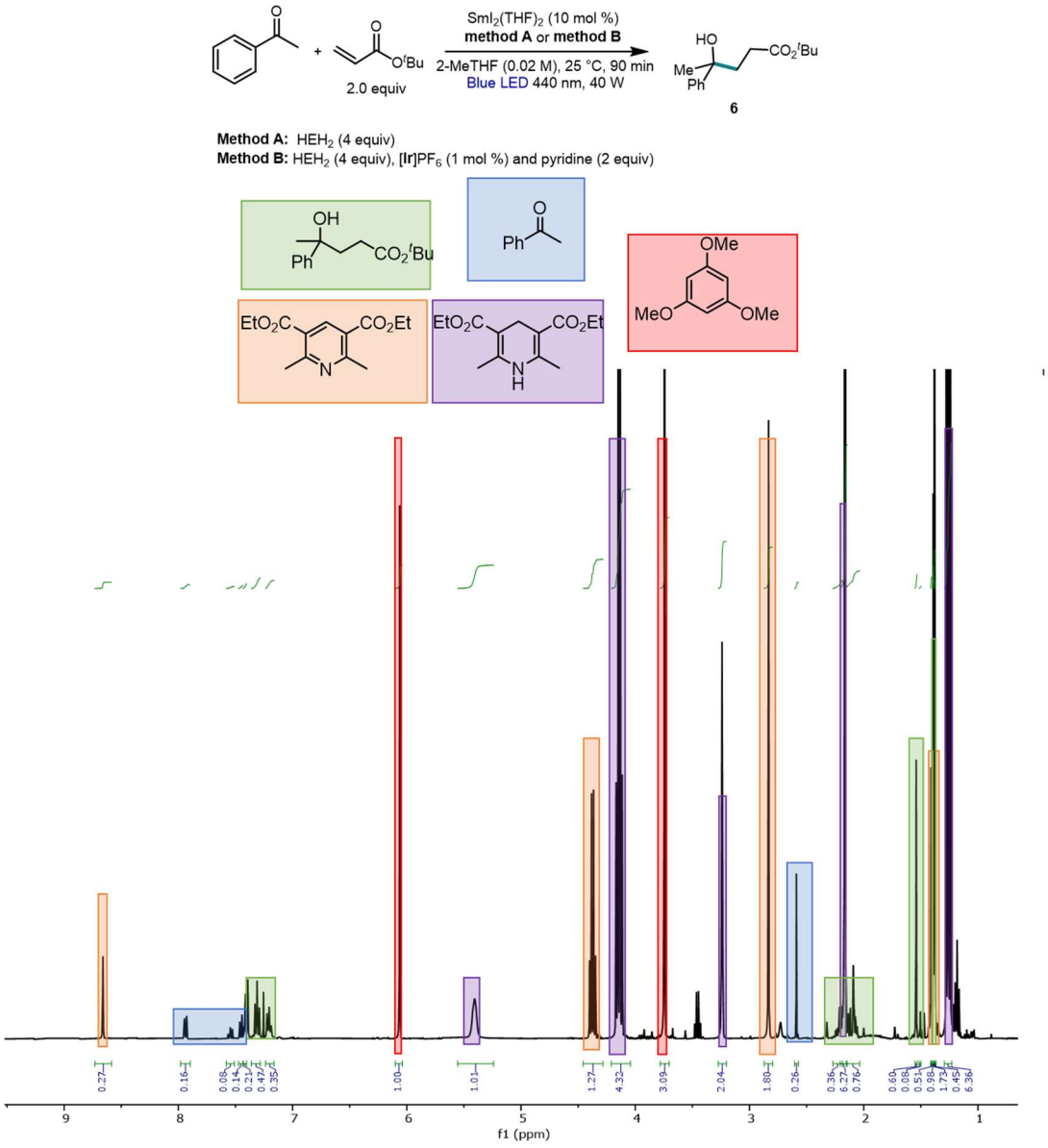

Figure E.7. ^{1}H NMR ($CDCl_3$ 7.26 ppm) of a typical crude reaction mixture reacting acetophenone with *tert*-butyl acrylate to produce 6 with key products/starting materials highlighted as indicated.

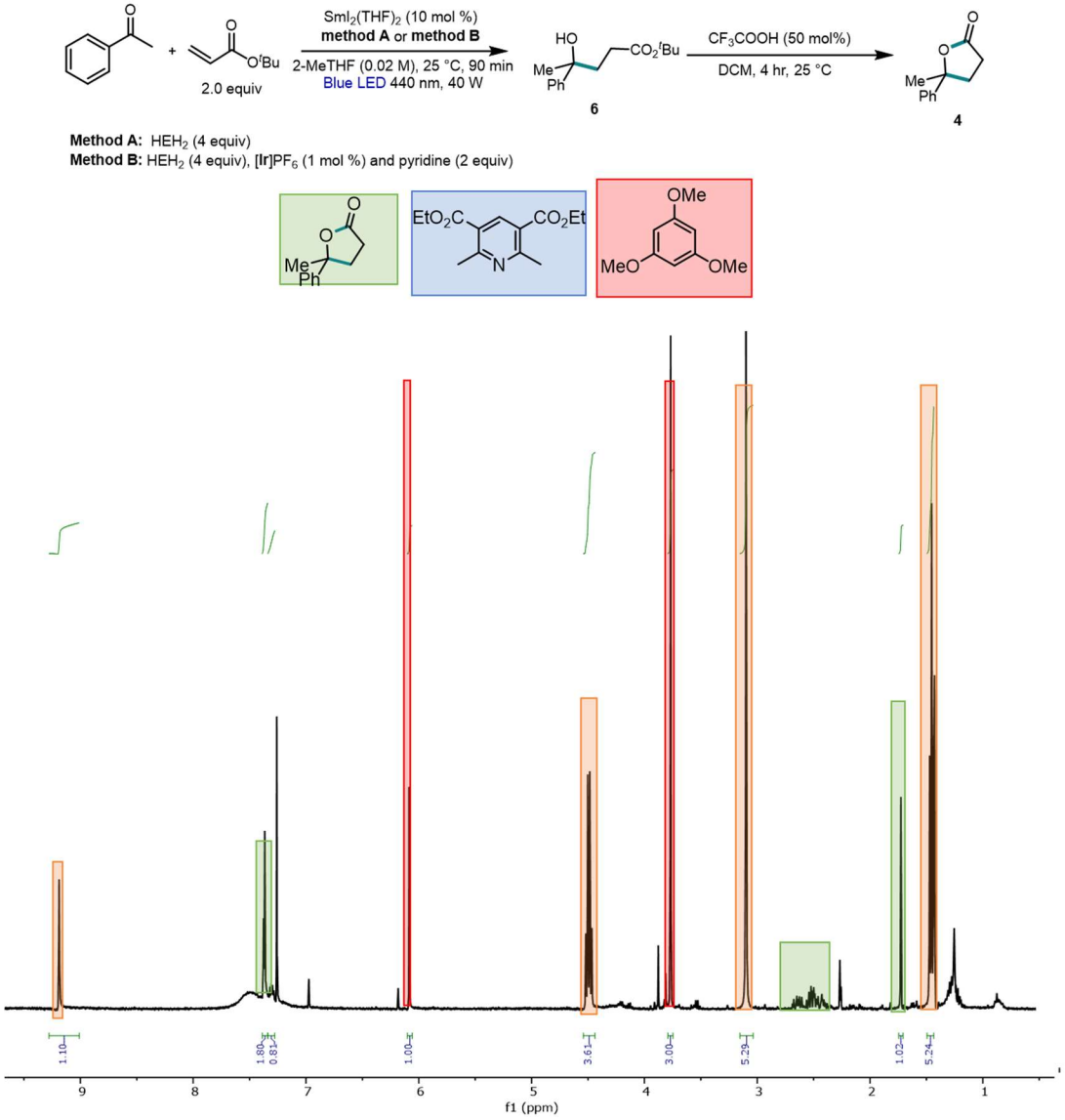

Figure E.8. ^{1}H NMR ($CDCl_3$ 7.26 ppm) of a typical crude reaction mixture reacting acetophenone with *tert*-butyl acrylate to produce 4 with key products/starting materials highlighted as indicated. The lactone product 4 matched previous reports.[5]

E.2.3 Additional catalysis tables

Table E.2. Additional catalytic experiments of ketone-acrylate coupling.

Method A: HEH_2 (4 equiv)
Method B: HEH_2 (4 equiv), **[Ir]**PF_6 (1 mol %) and pyridine (2 equiv)

Entry	Deviation	Yield (%) Method A	Yield (%) Method B
1	None	76	89
2	5.0 mol% Sm	58	79
3	2.5 mol% Sm	–	41
4	2 mL air added	4	32
5	1 equiv H_2O added	28	8
6	2 equiv Lutidine added (A)/instead of pyridine (B)	70	82
7	THF solvent	47	22
8	DBU instead of pyridine (B)	–	9
9	0 °C, 3 h	–	77
10	1 mmol scale, 0.05 M, 2 equiv HEH_2	–	89
11	1 mmol scale, 0.1 M, 2 equiv HEH_2, 6 h	–	61

Entry	12[a]	13[a]	14[b,c]
Product	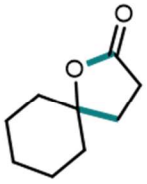	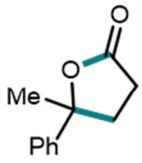	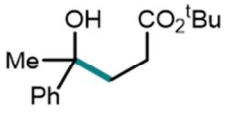
	3	4	6
method A:	30%	73%	36%
method B:	64%	83%	32%

[a]Ethyl acrylate instead of phenyl acrylate.
[b]*tert*-butyl acrylate instead of phenyl acrylate.
[c]1 equiv *tert*-butanol added.

Table E.3. Yields for pinacol coupled products in selected aryl ketone cross-coupling reactions.

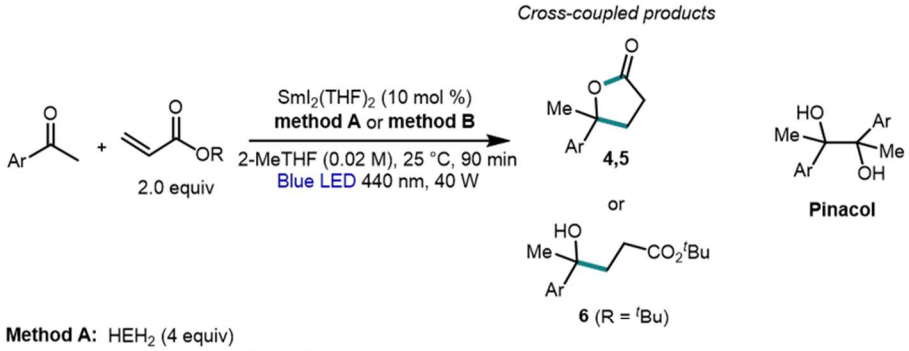

Method A: HEH_2 (4 equiv)
Method B: HEH_2 (4 equiv), **[Ir]**PF_6 (1 mol %) and pyridine (2 equiv)

Entry (Entry in Table 6.1)	Coupling partners and deviations	Product	Yield (%) Cross-coupling product Method A	Yield (%) pinacol product Method A (meso:dr)	Yield (%) Cross-coupling product Method B	Yield (%) pinacol product Method B (meso:dr)
1 (entry 13)	Ar = Ph, R = Ph	**4**	>95	–	90	8 (1:1)
2 (entry 14)	Ar = $^{4\text{-CF3}}$Ph, R = Ph	**5**	77	16 (0.6:1)	49	50 (0.8:1)
3 (entry 15)	Ar = Ph, R = ^{t}Bu	**6**	43	4 (0.4:1)	29	45 (0.7:1)
4	Ar = $^{4\text{-CF3}}$Ph, R = Ph; No Sm	–	–	15 (1:1)	–	100 (1:1)

Table E.4. Additional screening interrogating the effect of quencher (HEH_2, MeacrH, $phenH_2$, or Et_3N) on catalysis. All results with error bars represent the average and standard deviation of a minimum of two experiments.

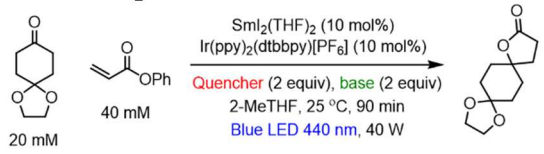

Entry	Quencher, base	Yield (%)	Recovered SM (%)
1	HEH_2, pyridine	64	~40
2	MeacrH, pyridine	52	0
3	HEH_2, lutidine	68	30
4	MeacrH, lutidine	45	~60
5	$phenH_2$, lutidine	71±2	17±2
6	Et_3N, Et_3N (1 mol% Ir)	8±1	70±2

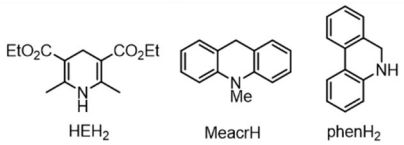

Table E.5. Additional screening interrogating the effects of additives (MgI_2 or [PyrH]TFSI) on catalysis.

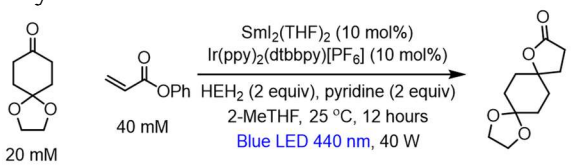

Entry	Variation	Yield (%)	Recovered SM (%)
1	None	64	~40
2	[PyrH]TFSI (2 equiv)	0	83
3	MgI_2 (1 equiv)	52	24
4	MgI_2 (1 equiv)/[PyrH]TFSI (2 equiv)	52	78
5	MeAcrH not HEH_2	52	0
6	MeAcrH instead of HEH_2; [PyrH]TFSI (2 equiv)	18	64
7	MeAcrH instead of HEH_2; MgI_2 (1 equiv)	25	39
8	MeAcrH instead of HEH_2; MgI_2 (1 equiv)/[PyrH]TFSI (2 equiv)	18	55

Table E.6. Additional screening interrogating the effect of HEH_2 loading on catalysis. All results with error bars represent the average and standard deviation of a minimum of two experiments.

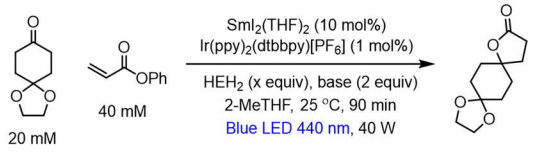

Entry	X equiv HEH_2, base	Yield (%)	Recovered SM (%)
1	2 equiv HEH_2, pyridine	70±3	4±1
2	4 equiv HEH_2, pyridine	89±1	6±1
3	1.2 equiv HEH_2, lutidine	46±6	48±6
4	2 equiv HEH_2, lutidine	68±3	22±2
5	4 equiv HEH_2, lutidine	82±1	12±1

E.3 UV-vis experiments

E.3.1 UV-vis detection of Sm interaction with dihydropyridines

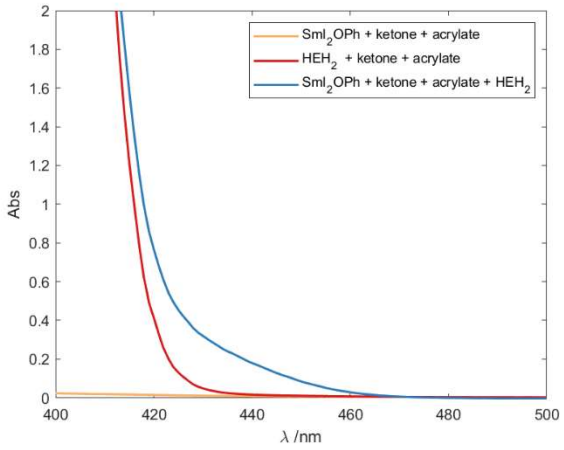

Figure E.9. Comparison of UV-vis traces (in a 1 mm path-length cuvette) of SmI_2 (2 mM) + ketone (20 mM) + acrylate (40 mM) (yellow trace, *in situ* forms colorless $Sm^{III}I_2(OPh)$); HEH_2 (80 mM) + ketone (20 mM) + acrylate (40 mM) (red trace); and SmI_2 (2 mM) + HEH_2 (80 mM) + ketone (20 mM) + acrylate (40 mM) (blue trace). All spectra collected in 2-MeTHF. Observed red-shift of the HEH_2 absorption in the presence of Sm^{III} is consistent with an interaction between species.

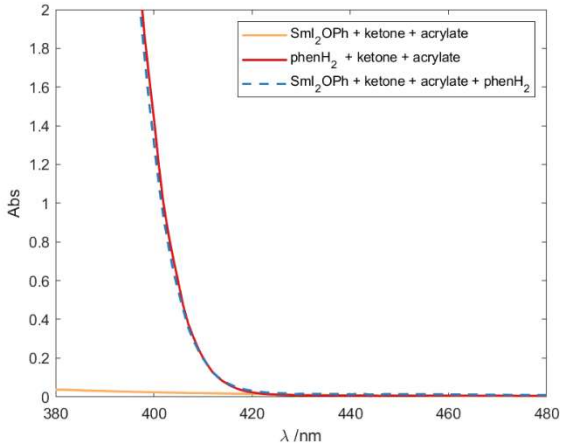

Figure E.10. Comparison of UV-vis traces (in a 1 mm path-length cuvette) of SmI_2 (2 mM) + ketone (20 mM) + acrylate (40 mM) (yellow trace, *in situ* forms colorless $Sm^{III}I_2(OPh)$); $phenH_2$ (80 mM) + ketone (20 mM) + acrylate (40 mM) (red trace); and SmI_2 (2 mM) + $phenH_2$ (80 mM) + ketone (20 mM) + acrylate (40 mM) (blue dashed trace).

All spectra collected in 2-MeTHF. Overlay suggests little to no interaction between Sm^{III} and $phenH_2$.

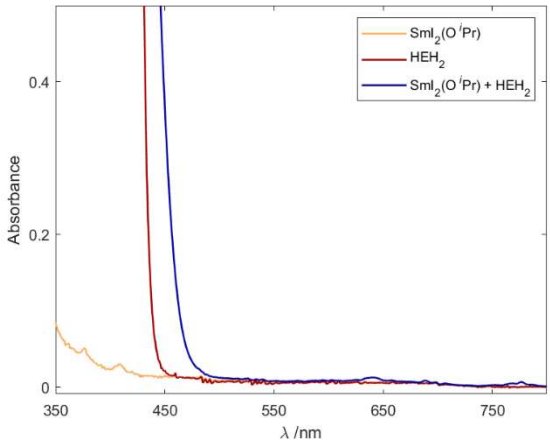

Figure E.11. Comparison of UV-vis traces (in a 1 cm path-length cuvette) of $Sm(O^iPr)_3$ (2 mM), $^nHep_4NI$ (6 mM), and HTFSI (3 mM) (yellow trace, *in situ* forms colorless $Sm^{III}I_2(O^iPr)$); HEH_2 (60 mM) (red trace); and $Sm(O^iPr)_3$ (2 mM), $^nHep_4NI$ (6 mM), HTFSI (3 mM), and HEH_2 (60 mM) (blue trace). All spectra collected in THF. The observed red-shift suggests interaction between Sm^{III} and HEH_2.

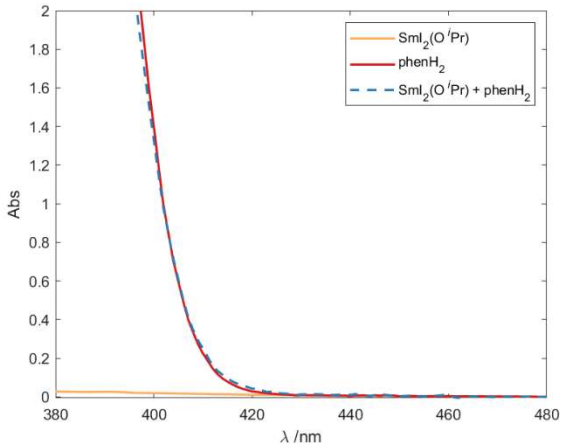

Figure E.12. Comparison of UV-vis traces (in a 1 mm path-length cuvette) of $Sm(O^iPr)_3$ (2 mM), $^nHep_4NI$ (6 mM), [LutH]TFSI (3 mM) (yellow trace, *in situ* forms colorless $Sm^{III}I_2(O^iPr)$); $phenH_2$ (60 mM) (red trace); and $Sm(O^iPr)_3$ (2 mM), $^nHep_4NI$ (6 mM), [LutH]TFSI (3 mM), and $phenH_2$ (60 mM) (dashed blue trace). All spectra collected in THF. Overlay suggests little to no interaction between Sm^{III} and $phenH_2$.

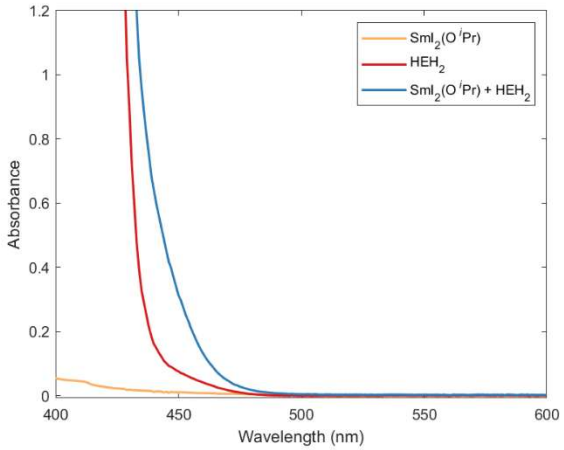

Figure E.13. Comparison of UV-vis traces (in a 1 cm path-length cuvette) of $Sm(O^iPr)_3$ (2 mM), ^{n}Hep$_4$NI (6 mM), [LutH]TFSI (3 mM) (yellow trace, *in situ* forms colorless $Sm^{III}I_2(O^iPr)$); HEH_2 (60 mM) (red trace); and $Sm(O^iPr)_3$ (2 mM), ^{n}Hep$_4$NI (6 mM), [LutH]TFSI (3 mM), and HEH_2 (60 mM) (blue trace). All spectra collected in THF. The observed red-shift suggests interaction between Sm^{III} and HEH_2.

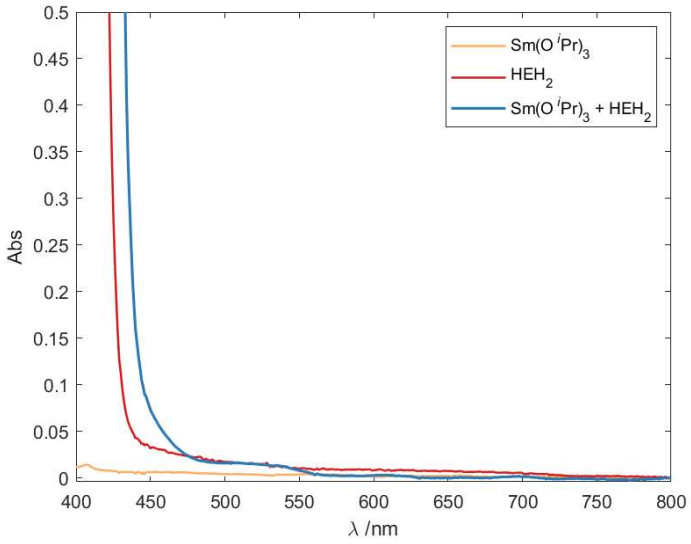

Figure E.14. Comparison of UV-vis traces (in a 1 cm path-length cuvette) of $Sm(O^iPr)_3$ (2 mM), ^{n}Hep$_4$NI (6 mM), (yellow trace, *in situ* is still colorless $Sm^{III}(O^iPr)_3$); HEH_2 (60 mM) (red trace); and $Sm(O^iPr)_3$ (2 mM), ^{n}Hep$_4$NI (6 mM), and HEH_2 (60 mM) (blue trace). All spectra collected in THF. The observed red-shift suggests interaction between Sm^{III} and HEH_2.

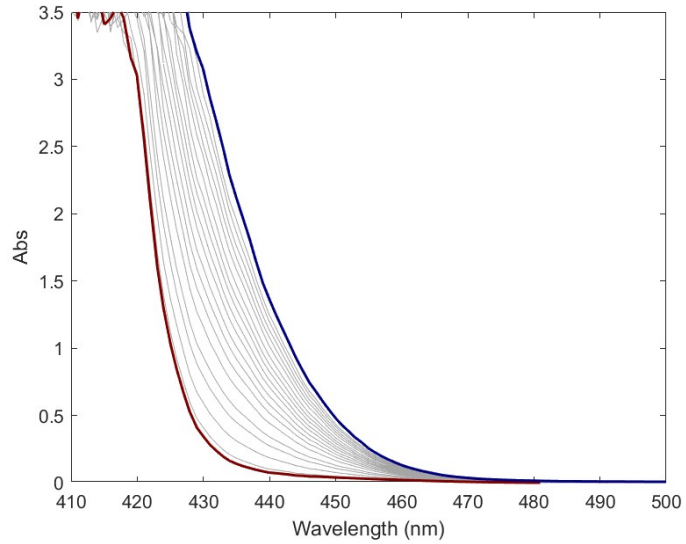

Figure E.15. Titration of $Sm(OTf)_3$ (0 to 5 mM, from red to blue trace) into a solution of HEH_2 (100 mM) in THF. Substantial red-shift observed upon titration of $Sm(OTf)_3$.

E.3.2 Sm^{II} photogeneration experiments

E.3.2.1 General procedure for Sm^{II} photogeneration experiments

A fresh 5 mM stock solution of SmI_2 in THF is prepared immediately before use. SmI_3 is prepared by titrating this 5 mM THF solution of SmI_2 with I_2 until the characteristic blue color of SmI_2 disappears.

An aliquot of the resulting SmI_3 solution (1 mL, 0.005 mmol) is added to a vial (1 mL) containing reductant (0.15 mmol, 30 equiv), and an additional 1 mL of THF, and this solution is transferred to a 1 cm path-length cuvette. 100 uL of a stock solution of photocatalyst is added to the cuvette, followed by base (0.15 mmol, 30 equiv), an additional 0.5 mL THF, and any alternative ligands (e.g., $^{n}Bu_4NBr$, BINAPO) as indicated.

E.3.2.2 General procedure for $Sm^{II}(HMPA)_4$ photogeneration experiments

For the $Sm^{II}(HMPA)^{2+}$ generation, 4 equiv HMPA was added to the isnitial SmI_2 solution prior to oxidation by I_2. The rest of the procedure was identical following E.3.2.1.

E.3.2.3 Summary of Sm^{II} photogeneration experiments

The Sm^{II} photogeneration experiments (S3.2.4) are summarized in Table E.7.

Table E.7. Summary of conditions and yields for photodriven Sm^{III} reductions. Approximate yield of Sm^{II} is determined based on the spectrum of the preparation of additive + SmI_2.

Sm^{III} + additives	**Photocat.**	**Conditions (THF and 25 °C unless otherwise specified)**	**Sm^{II} formation**
SmI_3 (2 mM)	-	HEH_2 (60 mM), Lut (60 mM), H150-Blue LED	~30%
SmI_3 (2 mM)	-	HEH_2 (60 mM), H160-440 nm LED	0%
$Sm(O^iPr)_3$ (2 mM), $^nHep_4NI$ (6 mM), HTFSI (3 mM)	-	HEH_2 (60 mM), H160-440 nm LED 40 W	~15%
$Sm(O^iPr)_3$ (2 mM), $^nHep_4NI$ (6 mM)	-	HEH_2 (60 mM), H160-440 nm LED 40 W	0%
SmI_3 (2 mM)	$[Ir]PF_6$ (0.2 mM)	HEH_2 (60 mM), Lut (60 mM), H160-440 nm LED 40 W	80%
SmI_3 (2 mM)	$[Ir]PF_6$ (0.2 mM)	HEH_2 (60 mM), H160-440 nm LED 40 W	10%
$Sm(O^iPr)_3$ (2 mM), $^nHep_4NI$ (6 mM), [LutH]TFSI (3 mM)	$[Ir]PF_6$ (0.2 mM)	HEH_2 (60 mM), Lut (60 mM), H160-440 nm LED 40 W	30%
SmI_3 (2 mM), $HO(CH_2)_2OH$ (2 mM)	$[Ir]PF_6$ (1 mM)	HEH_2 (60 mM), pyridine (60 mM), THF, 0 °C, H160-440 nm LED 40 W	15%
SmI_3 (2 mM), $MeO((CH_2)_2O)_3H$ (2 mM)	$[Ir]PF_6$ (1 mM)	HEH_2 (60 mM), pyridine (60 mM), THF, 0 °C,	5%
SmI_3 (2 mM), L* (2.2 mM)	$[Ir]PF_6$ (0.2 mM)	HEH_2 (60 mM), H160-440 nm LED 40 W	10%
SmI_3 (2 mM), $^nBu_4NBr$ (20 mM)	-	HEH_2 (60 mM), Lut (60 mM), H160-440 nm LED 40 W	0%
SmI_3 (2 mM), HMPA (8 mM)	-	HEH_2 (60 mM), Lut (60 mM), H160-440 nm LED 40 W	0%
SmI_3 (2 mM), $^nBu_4NBr$ (20 mM)	$[Ir]PF_6$ (0.2 mM)	Et_3N (60 mM), H160-440 nm LED 40 W	0%
SmI_3 (2 mM), HMPA (8 mM)	$[Ir]PF_6$ (0.2 mM)	Et_3N (60 mM), H160-440 nm LED 40 W	0%
SmI_3 (2 mM), BINAPO (2.2 mM)	$[Ir]PF_6$ (0.2 mM)	Et_3N (60 mM), H160-440 nm LED 40 W	0%
SmI_3 (2 mM)	3DPA2FBN (0.05 mM)	$acrH_2$ (60 mM) Et_3N (60 mM), H150-Blue LED 34 W	20%
SmI_3 (2 mM), $^nBu_4NBr$ (20 mM)	3DPA2FBN (0.05 mM)	$acrH_2$ (60 mM) Et_3N (60 mM), H160-440 nm LED 40 W	40%
SmI_3 (2 mM), HMPA (8 mM)	3DPA2FBN (0.05 mM)	$acrH_2$ (60 mM) Et_3N (60 mM), H150-Blue LED 34 W	10%
SmI_3 (2 mM), BINAPO (2.2 mM)	3DPA2FBN (0.05 mM)	$acrH_2$ (60 mM) Et_3N (60 mM), H160-440 nm LED 40 W	10%

S3.2.4 Sm^{II} photogeneration experiments

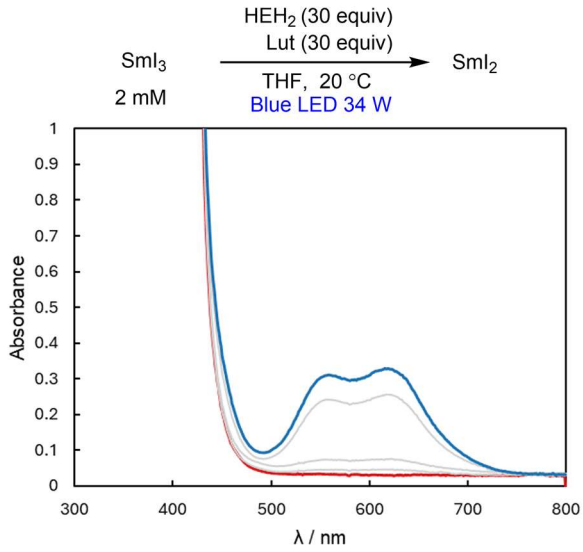

Figure E.16. Photogeneration of SmI_2 from a THF solution of SmI_3 (2 mM), HEH_2 (60 mM), and Lut (60 mM) on irradiation with H150-Blue LED; t = 0 (red trace); t =120 min (blue trace). Maximum intensity suggests about 30% conversion to SmI_2.

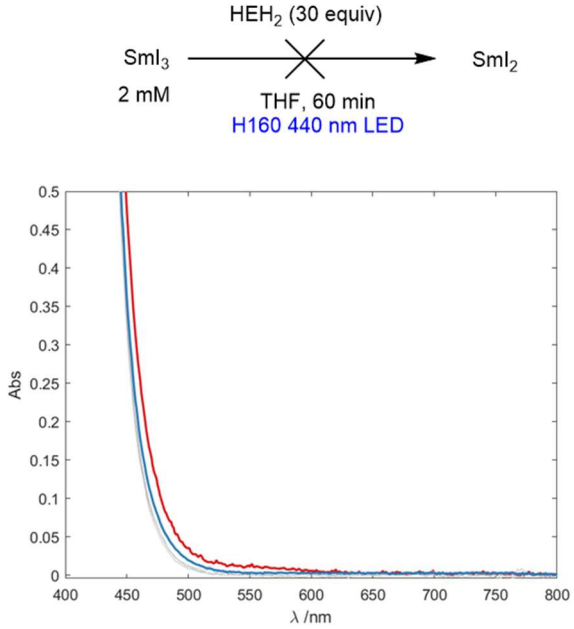

Figure E.17. Attempted photogeneration of SmI_2 from a THF solution of SmI_3 (2 mM) and HEH_2 (60 mM) on irradiation with H160-440 nm; t = 0 (red trace); t =60 min (blue trace). No SmI_2 is observed even on extended irradiation.

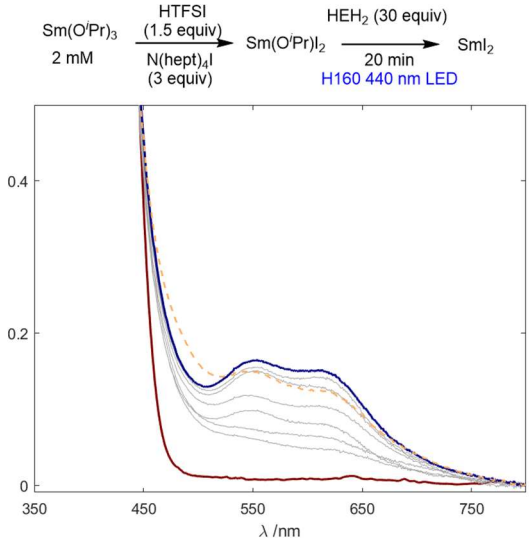

Figure E.18. Photogeneration of SmI_2 from a THF solution of $Sm(O^iPr)_3$ (2 mM), $^nHep_4NI$ (6 mM), HTFSI (3 mM), and HEH_2 (60 mM) on irradiation with H160 440 nm; t = 0 (red trace); t =20 min (lowest intensity grey trace), 80 minutes (blue trace), 180 minutes (yellow dashed trace) irradiation. Maximum intensity suggests about 15% conversion to SmI_2.

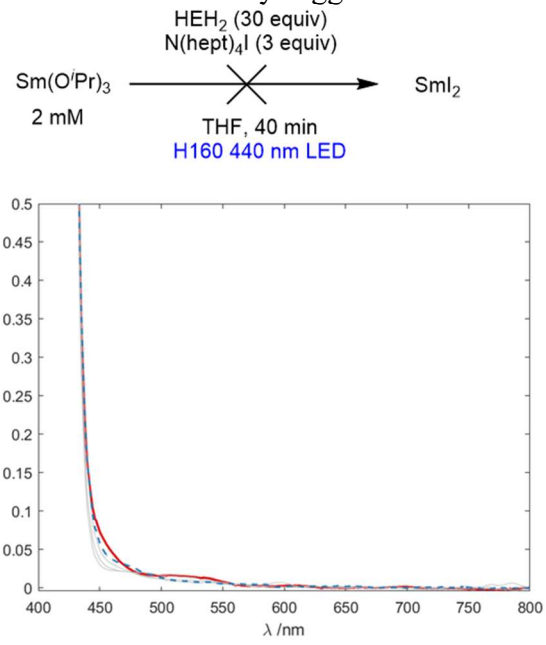

Figure E.19. Attempted photogeneration of SmI_2 from a THF solution of $Sm(O^iPr)_3$ (2 mM), $^nHep_4NI$ (6 mM), and HEH_2 (60 mM) on irradiation with H160-440 nm LED; t = 0 (red trace); t =40 min (blue dashed trace). No SmI_2 is observed even on extended irradiation.

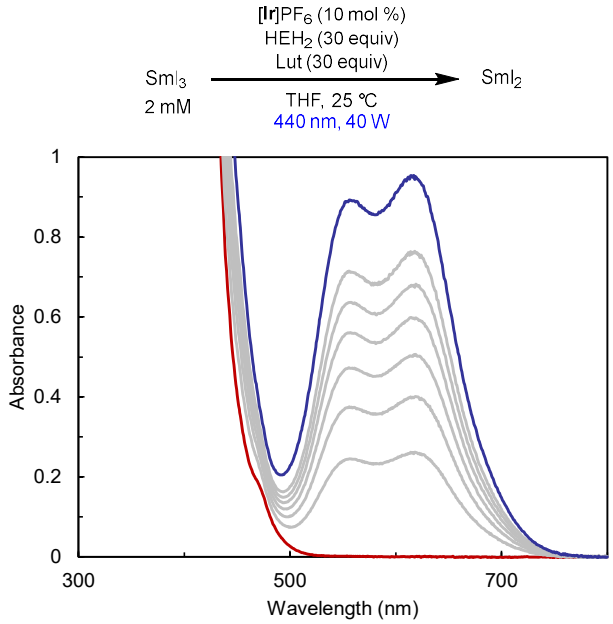

Figure E.20. Photogeneration of SmI_2 from a THF solution of SmI_3 (2 mM), HEH_2 (60 mM), and Lut (60 mM) with [Ir]PF_6 (0.2 mM) as photosensitizer on irradiation with H160-440 nm LED over t = 0 (red trace) to t = 2 min (blue trace). Maximum intensity suggests about 80% conversion to SmI_2.

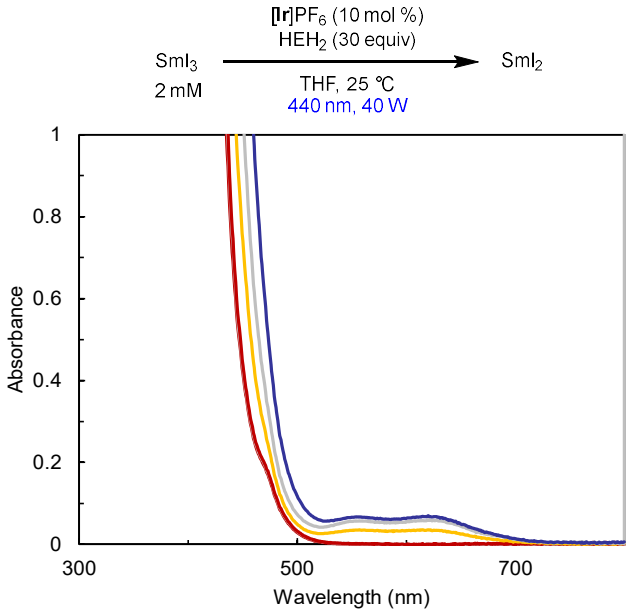

Figure E.21. Photogeneration of SmI_2 from a THF solution of SmI_3 (2 mM) and HEH_2 (60 mM) with [Ir]PF_6 (0.2 mM) as a photosensitizer in the absence of base on irradiation with H160-440 nm LED over t = 2 min (red trace), t = 6 min (yellow trace), to t = 16 min (dark blue trace). Maximum intensity suggests <10% conversion to SmI_2 over prolonged

irradiation; the absence of observed SmI_2 at 2 min (compared to 80% SmI_2 generation at the same time point in the presence of Lut) suggests that Lut accelerates SmI_2 photogeneration under these conditions.

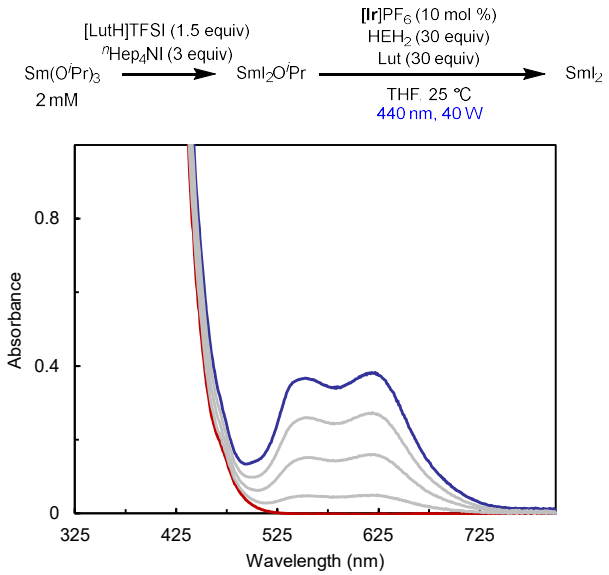

Figure E.22. Photogeneration of SmI_2 from a THF solution of $Sm(O^iPr)_3$ (2 mM), [LutH]TFSI (3 mM), $^nHep_4NI$ (6 mM), HEH_2 (60 mM), and Lut (60 mM) with $[Ir]PF_6$ (0.2 mM) as photosensitizer on irradiation with H160-440 nm LED over t = 0 (red trace) to t = 2 min (blue trace). Maximum intensity suggests ~30% conversion to SmI_2.

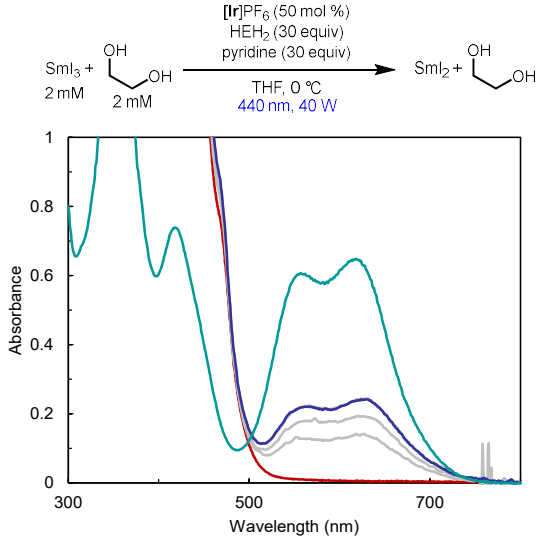

Figure E.23. Photogeneration of SmI_2 in the presence of ethylene glycol (2mM) from a THF solution of SmI_3 (2 mM), HEH_2 (60 mM), and pyridine (60 mM) with [Ir]PF_6 (1 mM) as photosensitizer on irradiation with H160-440 nm LED over t = 0 (red trace) to t = 2 min (dark blue trace). The Sm^{II} species that is generated has absorption maxima consistent with those of SmI_2 (1 mM) in the presence of ethylene glycol (1 mM) in THF (teal trace). Maximum intensity suggests ~15% steady state population of Sm^{II} under irradiation.

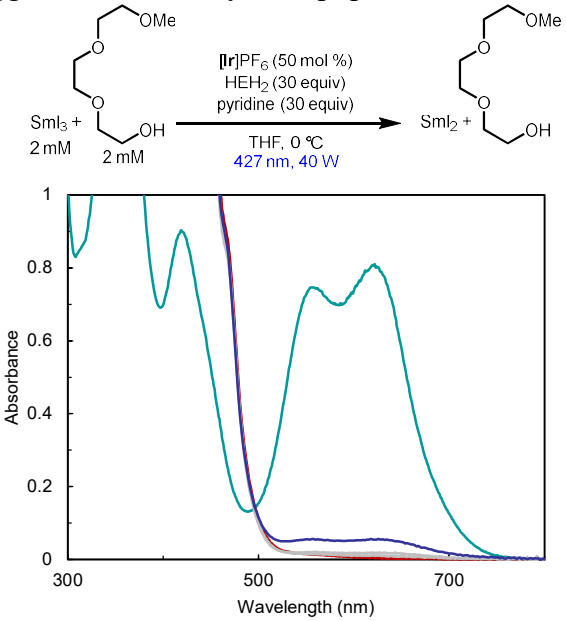

Figure E.24. Photogeneration of SmI_2 in the presence of $MeO((CH_2)_2O)_3H$ (2mM) from a THF solution of SmI_3 (2 mM), HEH_2 (60 mM), and pyridine (60 mM) with [Ir]PF_6 (1 mM) as photosensitizer on irradiation with H160-427 nm LED over t = 0 (red trace) to t = 30 min (dark blue trace). The Sm^{II} species that is generated has absorption maxima consistent

with those of SmI_2 (1 mM) in the presence of $MeO((CH_2)_2O)_3H$ (1 mM) in THF (teal trace). Maximum intensity suggests ~5% steady state population of Sm^{II} under irradiation.

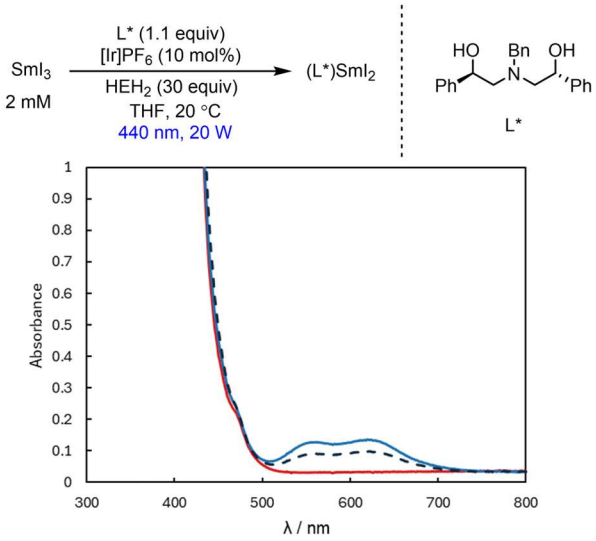

Figure E.25. Photogeneration and decay of SmI_2 from THF solution of SmI_3 (2 mM), L*(2.2 mM), $[Ir]PF_6$ (0.2 mM), HEH_2 (60 mM) on irradiation with H160-440 nm LED; t = 0 (red); t = 1 min (blue trace); t = 60 min (dashed). Maximum intensity suggests about 10% conversion to Sm^{II}. Note: the visible features of SmI_2 are unchanged in the presence of up to 2 equiv of L*, thus we are unable to assign the exact speciation of Sm(II) formed.

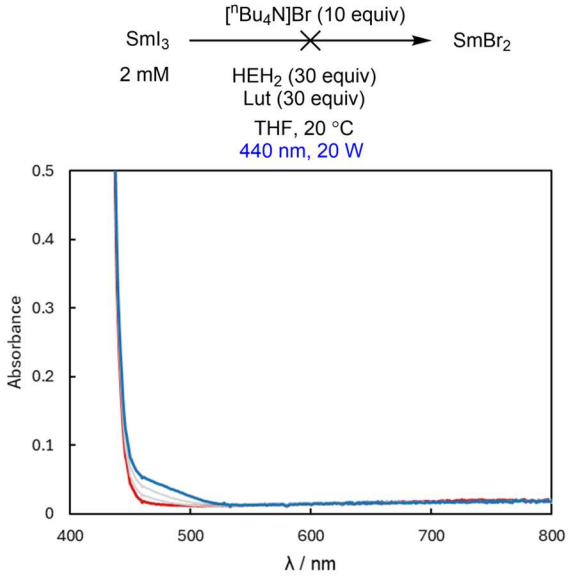

Figure E.26. Attempted photogeneration of $SmBr_2$ from a THF solution of SmI_3 (2 mM), $^{n}Bu_4NBr$ (20 mM), HEH_2 (60 mM), and Lut (60 mM) on irradiation with H160-440 nm LED; t = 0 (red trace); t = 60 min (blue trace). No $SmBr_2$ is observed.

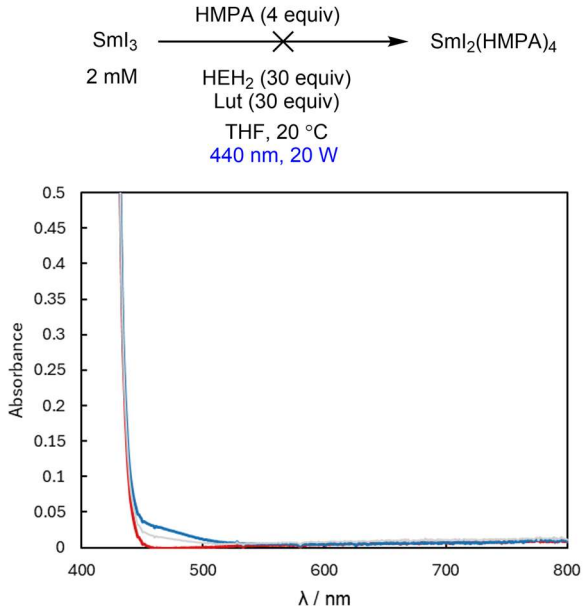

Figure E.27. Attempted photogeneration of $Sm(HMPA)_4^{2+}$ from a THF solution of SmI_3 (2 mM), HMPA (8 mM), HEH_2 (60 mM), and Lut (60 mM) on irradiation with H160-440 nm LED; t = 0 (red trace); t = 60 min (blue trace). No $Sm(HMPA)_4^{2+}$ is observed.

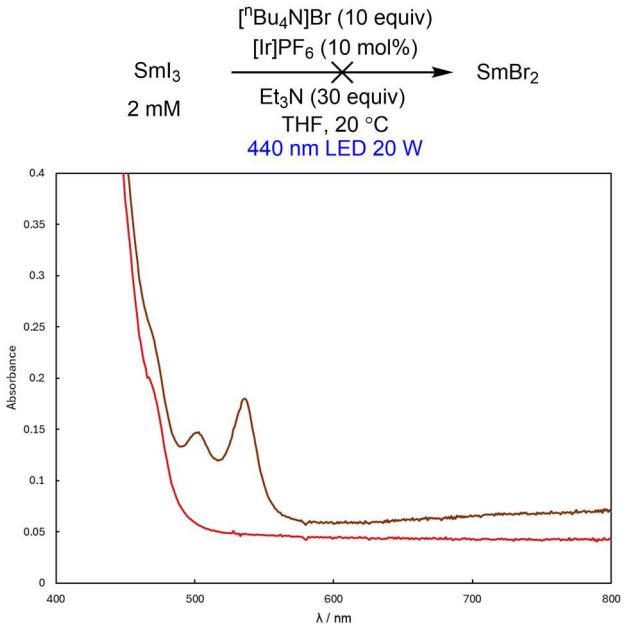

Figure E.28. Attempted photogeneration of $SmBr_2$ from a THF solution of SmI_3 (2 mM), $^{n}Bu_4NBr$ (20 mM), $[Ir(ppy)_2(dtbbpy)]PF_6$ (0.2 mM), and Et_3N (60 mM) on irradiation with H160-440 nm LED; t = 0 (red trace); t = 20 min (brown trace) shows formation of $[Ir^{II}(ppy)_2(dtbbpy)]$.[7] No $SmBr_2$ is observed.

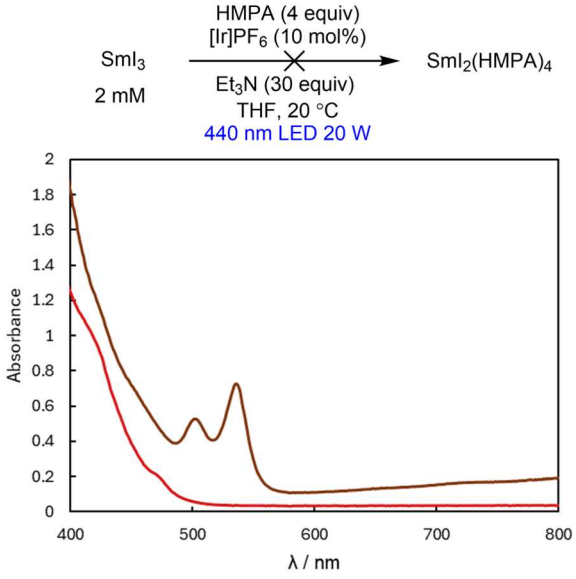

Figure E.29. Attempted photogeneration of $Sm(HMPA)_4^{2+}$ from a THF solution of SmI_3 (2 mM), HMPA (8 mM), $[Ir(ppy)_2(dtbbpy)]PF_6$ (0.2 mM), and Et_3N (60 mM) on irradiation

with H160-440 nm LED; t = 0 (red trace); t = 20 min (brown trace) shows formation of $[Ir^{II}(ppy)_2(dtbbpy)]$.[7] No $Sm(HMPA)_4^{2+}$ is observed.

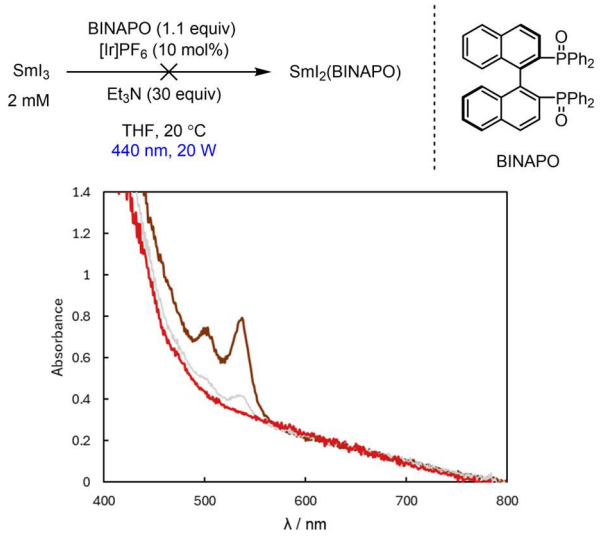

Figure E.30. Attempted photogeneration of $Sm(BINAPO)I_2$ from a THF solution of SmI_3 (2 mM), BINAPO (2.2 mM), $[Ir(ppy)_2(dtbbpy)]PF_6$ (0.2 mM), and Et_3N (60 mM) on irradiation with H160-440 nm LED; t = 0 (red trace); t = 20 min (brown trace) shows formation of $[Ir^{II}(ppy)_2(dtbbpy)]$.[7] No $Sm(BINAPO)I_2$ is observed.
Note: white solids precipitate from the solution, leading to poor transmission.

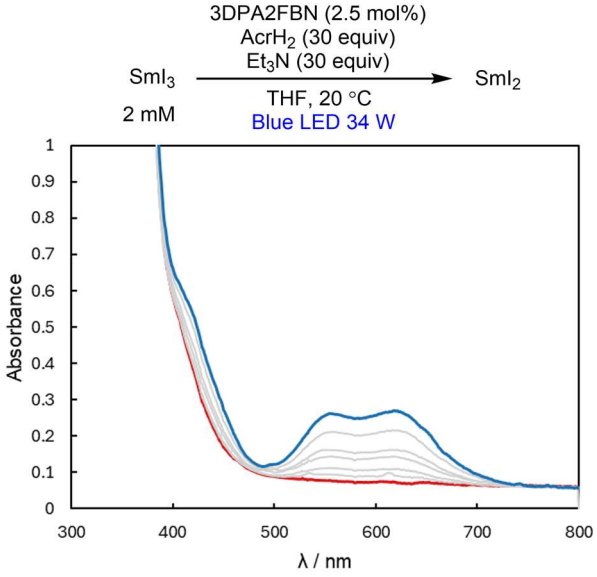

Figure E.31. Photogeneration of SmI_2 from a THF solution of SmI_3 (2 mM), 3DPA2FBN (0.05 mM), $AcrH_2$ (60 mM), and Et_3N (60 mM) on irradiation with H150-Blue LED; t = 0

(red trace); t =95 min (blue trace). Maximum intensity suggests about 20% conversion to SmI_2.

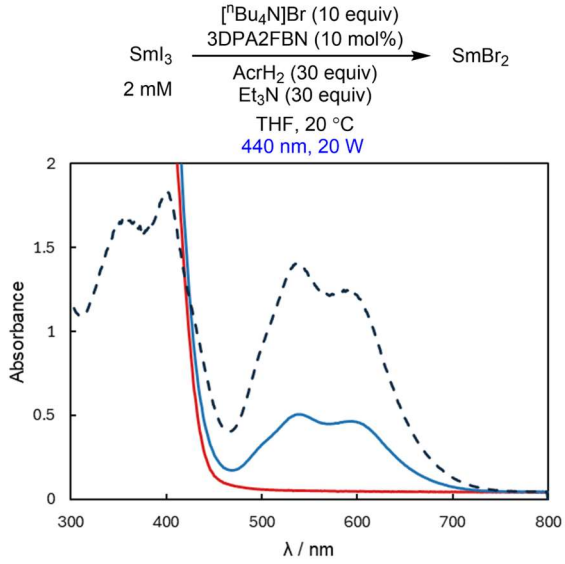

Figure E.32. Photogeneration of $SmBr_2$ from THF solution of SmI_3 (2 mM), $^nBu_4NBr$ (20 mM), 3DPA2FBN (0.2 mM), $AcrH_2$ (60 mM), and Et_3N (60 mM) on irradiation with H160-440 nm LED; t = 0 (red trace); t =1 min (blue trace); reference spectrum of 2 mM $SmBr_2$ (dashed trace). Maximum intensity (λ_{max} 588 nm and 540 nm) suggests about 40% conversion to $SmBr_2$.

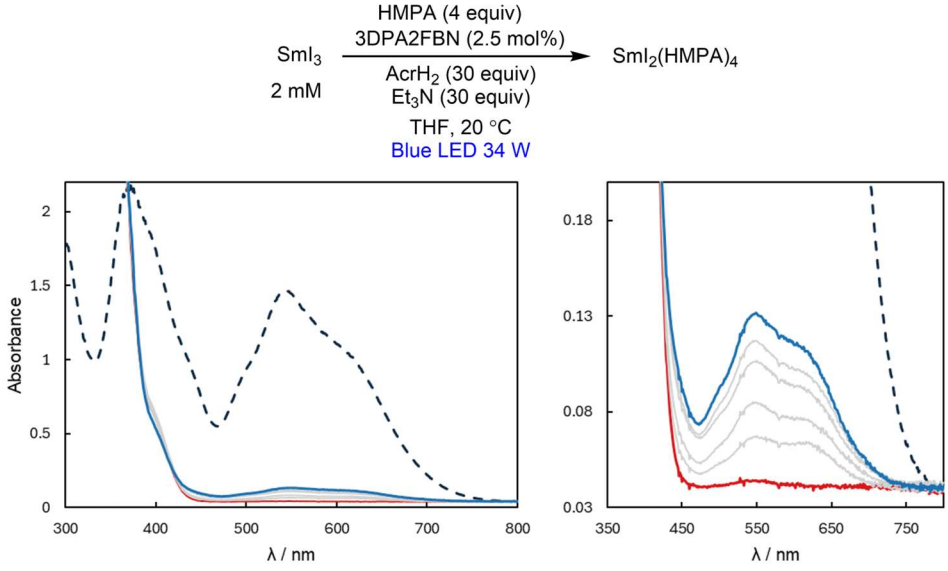

Figure E.33. Photogeneration of $SmI_2(HMPA)_4$ from THF solution of SmI_3 (2 mM), HMPA (8 mM), 3DPA2FBN (0.05 mM), $AcrH_2$ (60 mM), and Et_3N (60 mM) on irradiation

with H150-Blue LED; t = 0 (red); t = 60 min (blue). Rightmost plot shows magnified region of relevant Sm(II) absorbance. Maximum intensity (λ_{max} 540 nm) suggests about 10% conversion to $Sm(HMPA)_4I_2$.

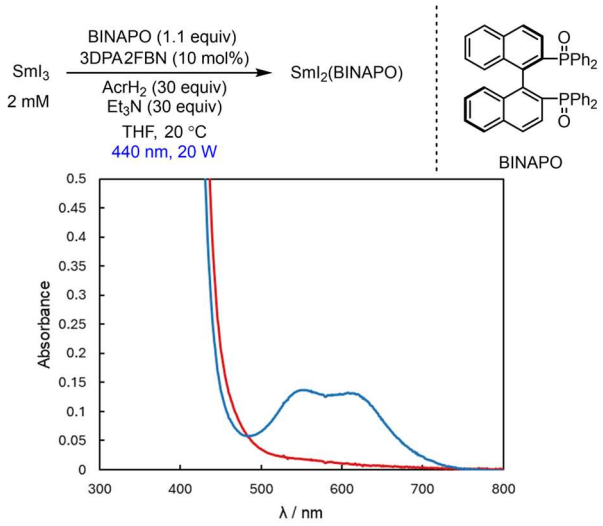

Figure E.34. Photogeneration of $Sm(BINAPO)I_2$ from THF solution of SmI_3 (2 mM), BINAPO (2.3 mM), 3DPA2FBN (0.2 mM), $AcrH_2$ (60 mM), and Et_3N (60 mM) on irradiation with H160-440 nm LED; t = 0 (red); t = 2 min (blue). Maximum intensity (λ_{max} = 550 nm and 608 nm) suggests about 10% conversion to $Sm(BINAPO)I_2$.

E.4 Electrochemical measurements

Comment on $Sm^{III/II}$ reduction potentials: The solution-phase speciation of SmX_n is ill-defined and highly dependent on the concentration of both Sm and potential ligands. As a result, rigorous definition of $Sm^{III/II}$ redox potentials for discrete species is nontrivial. Cyclic voltammetry of SmI_3 in THF is illustrative of this issue. As shown in Figure E.35, the observed $E_{1/2}$ of the reversible $Sm^{III/II}$ couple of $SmI_3(THF)_n$ (using a tetraalkylammonium triflimide salt as a relatively innocent supporting electrolyte) shifts negative by 59 mV per decade increase in ^{n}Hep$_4$NI concentration. This behavior is consistent with reversible dissociation of I^- upon reduction, with the position of the wave described by the Nernst eqn E.1:

$$E_{1/2} = E° - \frac{RT}{F} \ln([I^-]) \text{ (eqn E.1).}$$

The standard potential $E°(SmI_3/SmI_2 + I^-)$, which can be extrapolated from the intercept of a plot of $E_{1/2}$ vs $-\log[I^-]$ as −1.58 V vs $Fc^{+/0}$, is therefore only equivalent to the $E_{1/2}$ observed by CV if $[I^-] = 1$ M.

Despite this challenge, knowledge of the electrochemical properties of Sm species in the presence of various additives is useful in guiding selection of appropriate photoreductants and photoredox catalysts for Sm^{III} reduction. For the purpose of this study, we have collected CV data under a unified set of conditions, using concentrations of Sm and additives relevant to the UV-Vis studies of Sm^{II} generation. It should be emphasized, however, that the observed reduction potentials in these specific cocktails must not be treated as diagnostic standard reduction potentials for discrete $Sm^{II}L_n$ species.

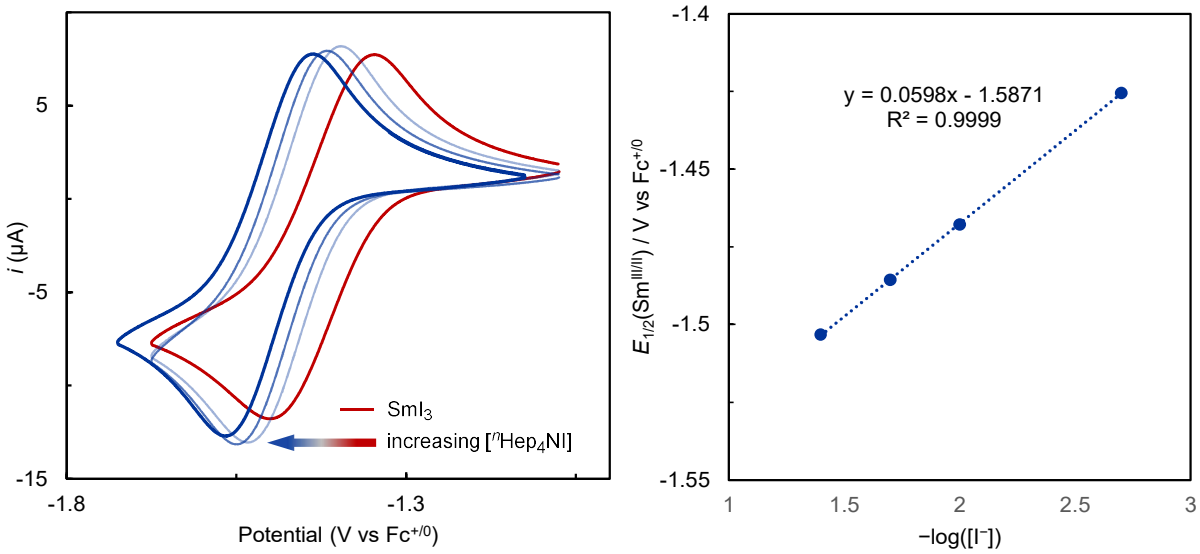

Figure E.35. Left: CVs of SmI_3 (2 mM) in the presence of 0-40 mM ^{n}Hep$_4$NI (red-dark blue traces) in THF containing 0.1 M BMPipTFSI at 25 mV s^{-1}. Right: plot of $E_{1/2}$ values from each CV vs $-\log([I^-])$.

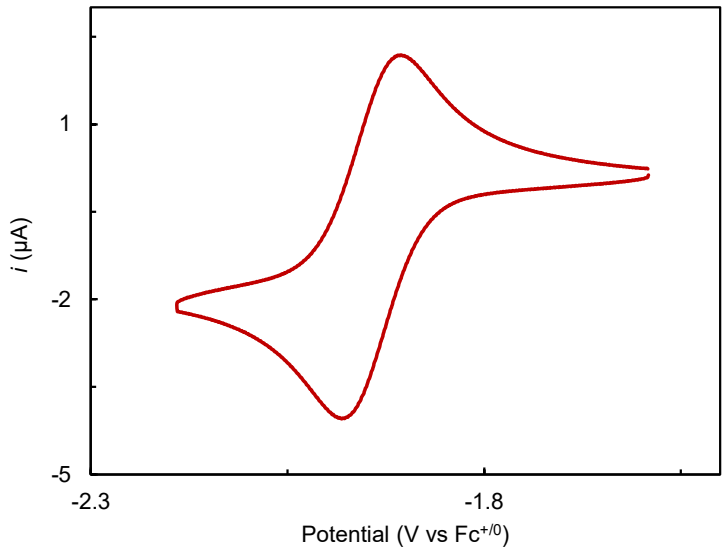

Figure E.36. CV of [Ir]PF_6 (0.5 mM) in THF containing 0.1 M BMPipTFSI at 25 mV s^{-1}.

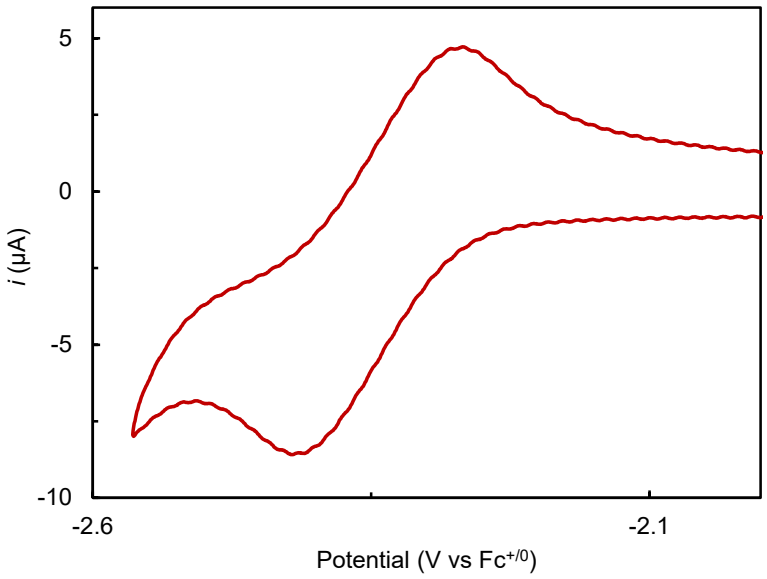

Figure E.37. CV of 3DPA2FBN (1 mM) in THF containing 0.1 M BMPipTFSI at 100 mV s^{-1}.

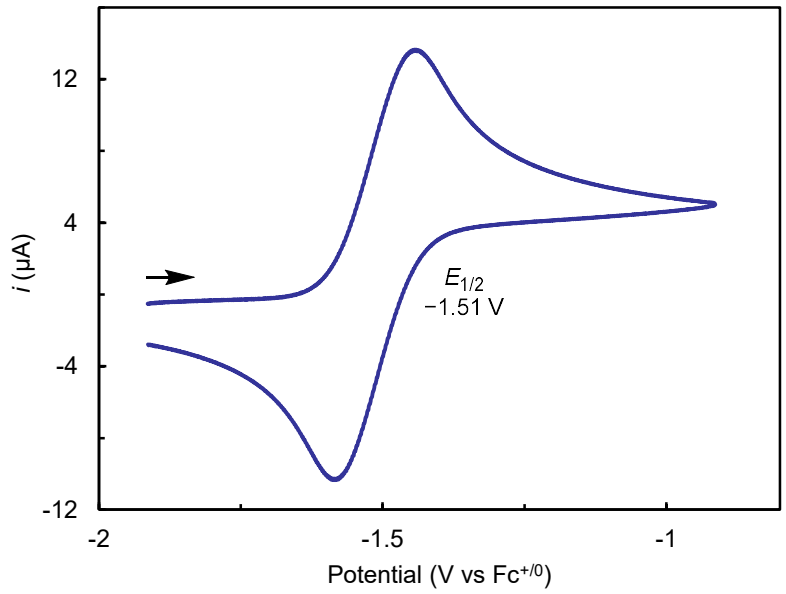

Figure E.38. CV of SmI_2 (2 mM) and $^{n}Hep_4NI$ (10 mM) in THF containing 0.1 M BMPipTFSI at 25 mV s^{-1}.

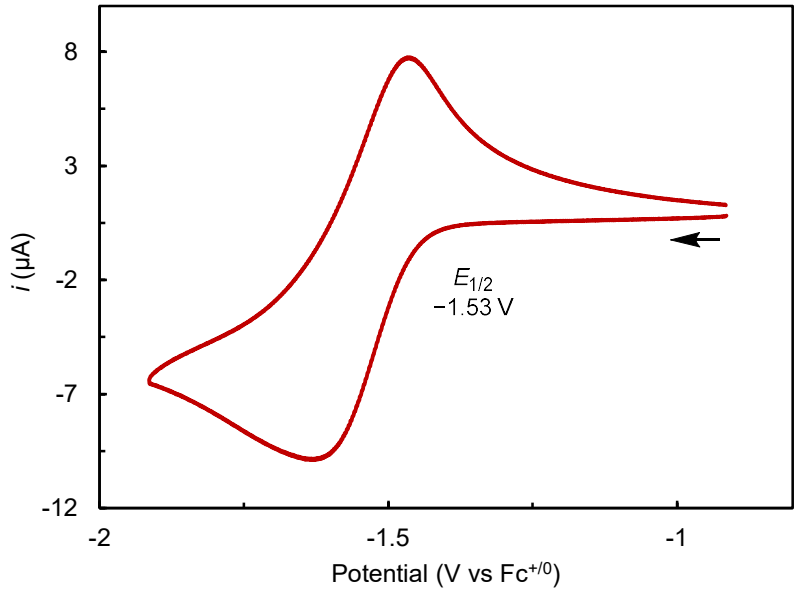

Figure E.39. CV of SmI_3 (2 mM), $^{n}Hep_4NI$ (10 mM), and ethylene glycol (2 mM) in THF containing 0.1 M BMPipTFSI at 25 mV s^{-1}.

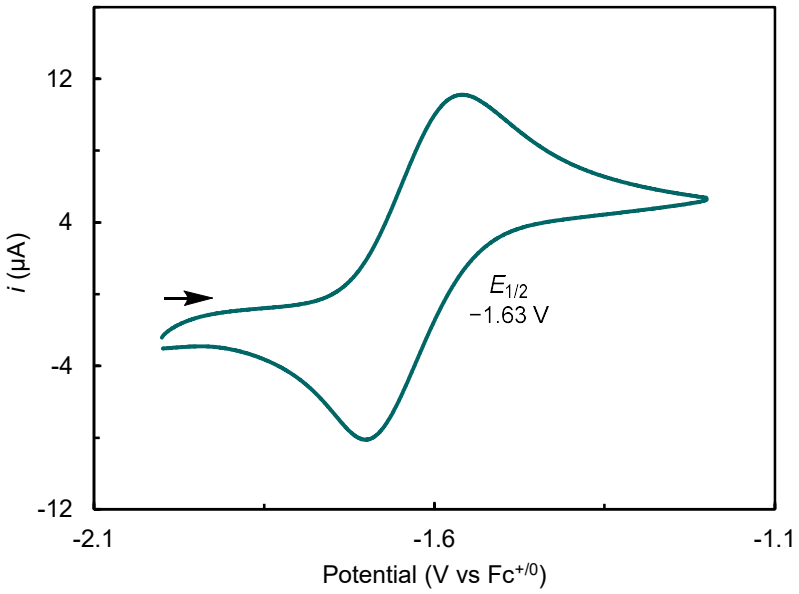

Figure E.40. CV of SmI_2 (2 mM), $^{n}Hep_4NI$ (10 mM), and $MeO((CH_2)_2O)_3H$ (2 mM) in THF containing 0.1 M BMPipTFSI at 25 mV s^{-1}.

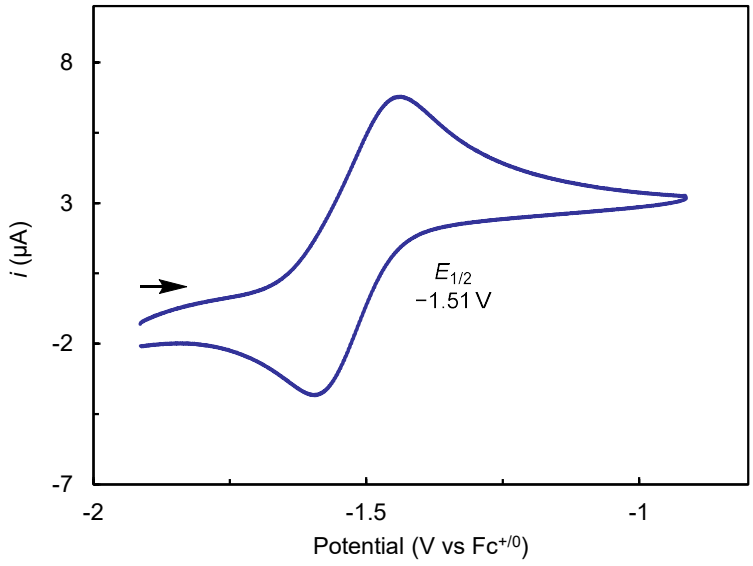

Figure E.41. CV of SmI_2 (2 mM), $^{n}Hep_4NI$ (10 mM), and 3-aza-3-benzyl-1(R),5,(R)-dihydroxy-1,5-diphenylpentane (2 mM) in THF containing 0.1 M BMPipTFSI at 25 mV s^{-1}.

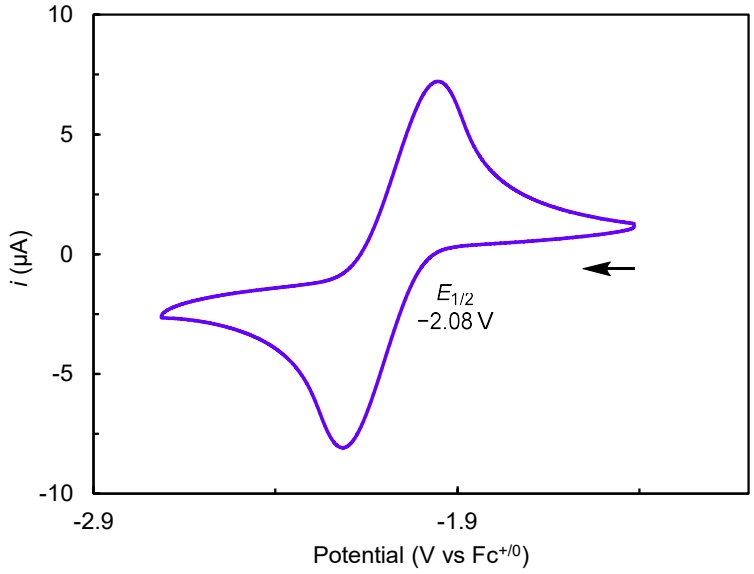

Figure E.42. CV of SmI_3 (2 mM) and $^{n}Bu_4NBr$ (20 mM) in THF containing 0.1 M BMPipTFSI at 25 mV s^{-1}.

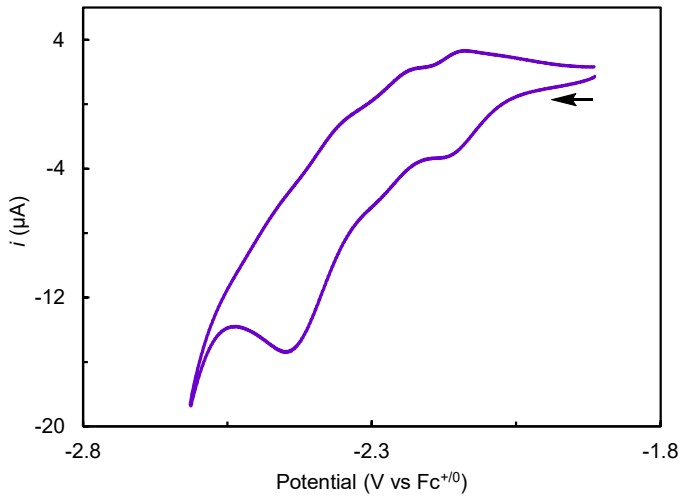

Figure E.43. CV of SmI_2 (2 mM), $^{n}Hep_4NI$ (10 mM), and BINAPO (2 mM) in THF containing 0.1 M BMPipTFSI at 25 mV s^{-1}. The speciation of this mixture is clearly complex. However, the observation that the more reducing photocatalyst 3DPA2FBN is

required to generate Sm^{II} species in the presence of BINAPO is consistent with the observation of $Sm^{III/II}$ redox waves negative of −2 V.

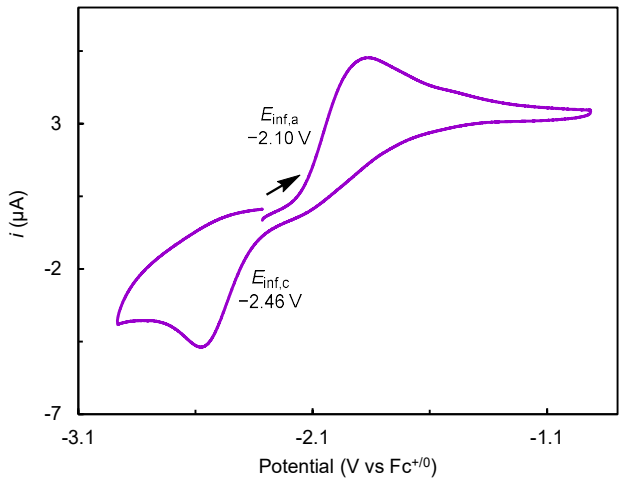

Figure E.44. CV of SmI_2 (2 mM) and HMPA (8 mM) in THF containing 0.1 M BMPipTFSI at 25 mV s^{-1}.

E.5 Additional mechanistic schemes

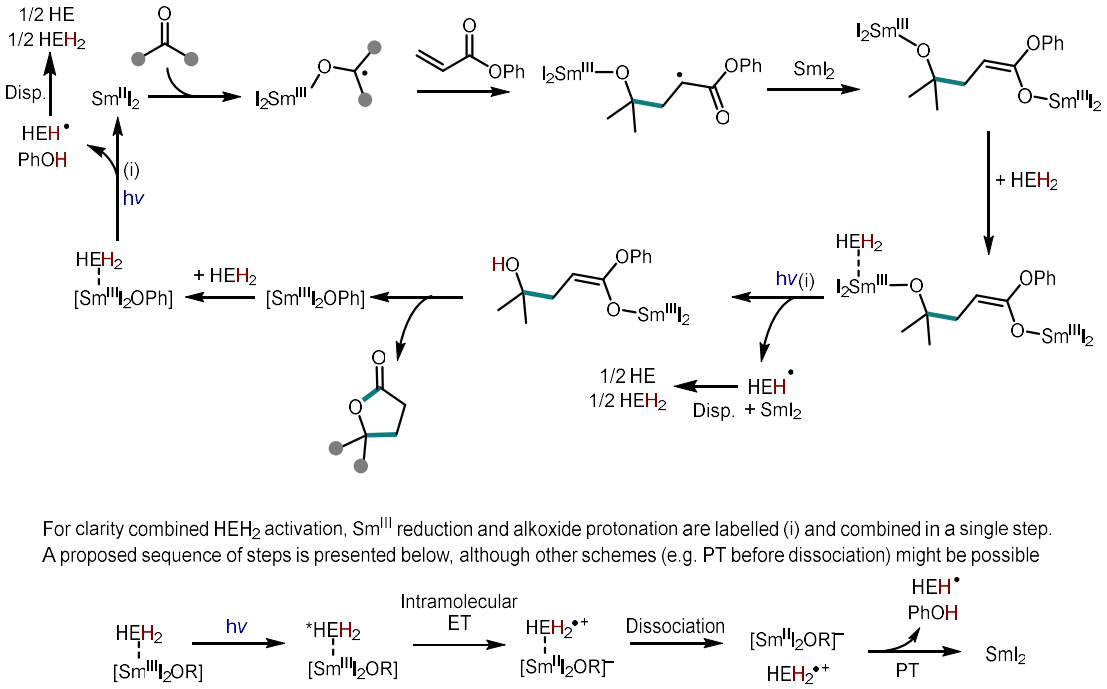

For clarity combined HEH_2 activation, Sm^{III} reduction and alkoxide protonation are labelled (i) and combined in a single step. A proposed sequence of steps is presented below, although other schemes (e.g. PT before dissociation) might be possible

Figure E.45. An alternative scheme for catalytic ketone-acrylate coupling reaction where HEH• does not terminate radical and two equivalents of SmI_2 are required per reduction.

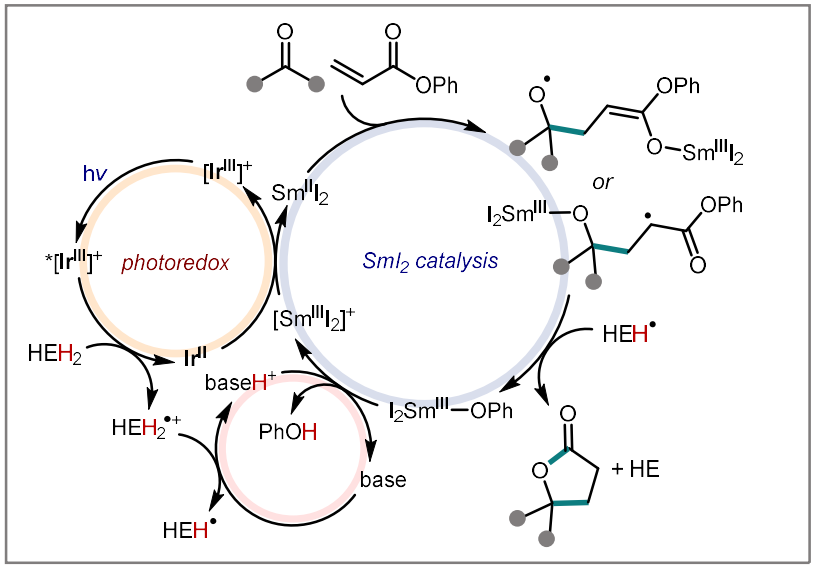

Figure E.46. A scheme for catalytic ketone-acrylate coupling reaction with $[Ir]^+$. Sm^{III}-OPh is regenerated as depicted in Figure 6.3B in chapter 6.

E.6 References for Appendix E

1. Watson, P. L.; Tulip, T. H.; Williams, I. *Organometallics* **1990**. 9, 1999–2009.
2. Matesic, L.; Locke, J. M.; Vine, K. L.; Ranson, M.; Bremner, J. B.; Skropeta, D. *Tetrahedron* **2012**. 68, 6810–6819.
3. Seki, T.; McEleney, K.; Crudden, C. M. *Chem. Commun.* **2012**. 48, 6369–6371.
4. Evans, D. A.; Nelson, S. G.; Gagne, M. R.; Muci, A. R. *J. Am. Chem. Soc.* **1993**. 115, 9800–9801.
5. Boyd, E. A.; Shin, C.; Charboneau, D. J.; Peters, J. C.; Reisman, S. E. *Science* **2024**. 385, 837-843.
6. Norcross, B. E.; Clement, G.; Weinstein, M. *J. Chem. Educ.* **1969**. 46, 694.
7. Baek, Y.; Reinhold, A.; Tian, L.; Jeffrey, P. D.; Scholes, G. D.; Knowles, R. R. *J. Am. Chem. Soc.* **2023**. 145, 12499–12508.